

DEVELOPMENT AND VALIDATION OF A VERTICALLY  
TWO-DIMENSIONAL MESOSCALE NUMERICAL MODEL(U) AIR FORCE  
INST OF TECH WRIGHT-PATTERSON AFB OH M K WALTERS  
AUG 85 AFIT/CI/NR-85-105T F/G 4/2

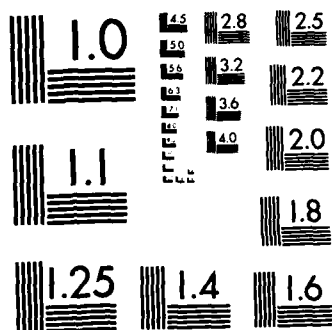
HL

UNCLASSIFIED

AUG 85 AFIT/CI/NR-85-105T

F/G 4/2

END  
FILMED  
ORC



MICROCOPY RESOLUTION TEST CHART  
NATIONAL BUREAU OF STANDARDS-1963-A

UNCLASS

SECURITY CLASSIFICATION OF THIS PAGE (When Data Entered)

## REPORT DOCUMENTATION PAGE

READ INSTRUCTIONS  
BEFORE COMPLETING FORM

1. REPORT NUMBER

AFIT/CI/NR 85-105T

2. GOVT ACCESSION NO.

AD-A160 741

3. RECIPIENT'S CATALOG NUMBER

4. TITLE (and Subtitle)

Development and Validation of a Vertically  
Two-Dimensional Mesoscale Numerical  
Model

5. TYPE OF REPORT &amp; PERIOD COVERED

THESIS/DISSERTATION

6. PERFORMING ORG. REPORT NUMBER

7. AUTHOR(s)

Michael Kent Walters

8. CONTRACT OR GRANT NUMBER(s)

9. PERFORMING ORGANIZATION NAME AND ADDRESS

AFIT STUDENT AT: Texas A&amp;M University

10. PROGRAM ELEMENT, PROJECT, TASK  
AREA & WORK UNIT NUMBERS

11. CONTROLLING OFFICE NAME AND ADDRESS

AFIT/NR  
WPAFB OH 45433 - 6583

12. REPORT DATE

Aug 1985

13. NUMBER OF PAGES

66

14. MONITORING AGENCY NAME &amp; ADDRESS (if different from Controlling Office)

15. SECURITY CLASS. (of this report)

UNCLASS

15a. DECLASSIFICATION/DOWNGRADING  
SCHEDULE

16. DISTRIBUTION STATEMENT (of this Report)

APPROVED FOR PUBLIC RELEASE; DISTRIBUTION UNLIMITED

DTIC  
ELECTE

OCT 30 1985

17. DISTRIBUTION STATEMENT (of the abstract entered in Block 20, if different from Report)

B

18. SUPPLEMENTARY NOTES

APPROVED FOR PUBLIC RELEASE: IAW AFR 190-1

*Lynn E. Wolaver*  
 LYNN E. WOLAVER 30481  
 Dean for Research and  
 Professional Development  
 AFIT, Wright-Patterson AFB OH

19. KEY WORDS (Continue on reverse side if necessary and identify by block number)

20. ABSTRACT (Continue on reverse side if necessary and identify by block number)

ATTACHED

DD FORM 1473

1 JAN 73

EDITION OF 1 NOV 65 IS OBSOLETE

UNCLASS

SECURITY CLASSIFICATION OF THIS PAGE (When Data Entered)

AD-A160 741

DTIC FILE COPY

## AFIT RESEARCH ASSESSMENT

The purpose of this questionnaire is to ascertain the value and/or contribution of research accomplished by students or faculty of the Air Force Institute of Technology (AFIT). It would be greatly appreciated if you would complete the following questionnaire and return it to:

AFIT/NR  
Wright-Patterson AFB OH 45433

SEARCH TITLE: Development and Validation of a Vertically Two-Dimensional Mesoscale Numerical Model

THOR: Michael Kent Walters

## SEARCH ASSESSMENT QUESTIONS:

1. Did this research contribute to a current Air Force project?

☐ a. YES

☐ b. NO

2. Do you believe this research topic is significant enough that it would have been researched (or contracted) by your organization or another agency if AFIT had not?

☐ a. YES

☐ b. NO

3. The benefits of AFIT research can often be expressed by the equivalent value that your agency achieved/received by virtue of AFIT performing the research. Can you estimate what this research would have cost if it had been accomplished under contract or if it had been done in-house in terms of manpower and/or dollars?

☐ a. MAN-YEARS \_\_\_\_\_

☐ b. \$ \_\_\_\_\_

4. Often it is not possible to attach equivalent dollar values to research, although the results of the research may, in fact, be important. Whether or not you were able to establish an equivalent value for this research (3. above), what is your estimate of its significance?

☐ a. HIGHLY  
SIGNIFICANT

☐ b. SIGNIFICANT

☐ c. SLIGHTLY  
SIGNIFICANT

☐ d. OF NO  
SIGNIFICANCE

5. AFIT welcomes any further comments you may have on the above questions, or any additional details concerning the current application, future potential, or other value of this research. Please use the bottom part of this questionnaire for your statement(s).

NAME	GRADE	POSITION
ORGANIZATION	LOCATION	

STATEMENT(s):

FOLD DOWN ON OUTSIDE - SEAL WITH TAPE

AFIT/NR  
WRIGHT-PATTERSON AFB OH 45433  
OFFICIAL BUSINESS  
PENALTY FOR PRIVATE USE. \$300



NO POSTAGE  
NECESSARY  
IF MAILED  
IN THE  
UNITED STATES



**BUSINESS REPLY MAIL**

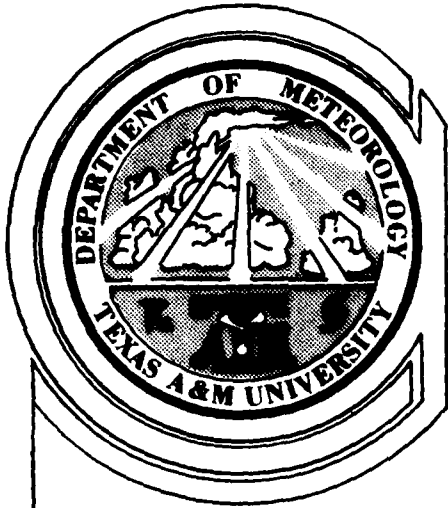
FIRST CLASS PERMIT NO. 73236 WASHINGTON D.C.

POSTAGE WILL BE PAID BY ADDRESSEE

AFIT/ DAA  
Wright-Patterson AFB OH 45433

FOLD IN

①



**TEXAS A & M UNIVERSITY**

**DEPARTMENT OF  
METEOROLOGY**

# **Development and Validation of a Vertically Two-Dimensional Mesoscale Numerical Model**

by  
**Michael Kent Walters**

**August 1985**



85 10 30 058

DEVELOPMENT AND VALIDATION OF A VERTICALLY  
TWO-DIMENSIONAL MESOSCALE NUMERICAL MODEL

A Thesis

by

MICHAEL KENT WALTERS

Submitted to the Graduate College of  
Texas A&M University  
in partial fulfillment of the requirement for the degree of  
MASTER OF SCIENCE

August 1985

Major Subject: Meteorology



Accepted For	
Major Subject	<input checked="checked" type="checkbox"/>
Minor Subject	<input type="checkbox"/>
Thesis	<input type="checkbox"/>
Abstract	
Indexing	
Publication	
Approval by Codes	
Signature	
Date	

DEVELOPMENT AND VALIDATION OF A VERTICALLY  
TWO-DIMENSIONAL MESOSCALE NUMERICAL MODEL

A Thesis

by

MICHAEL KENT WALTERS

Approved as to style and content by:

Dusan Djuric

Dusan Djuric  
(Chair of Committee)

Kenneth C. Brundidge

Kenneth C. Brundidge  
(Member)

David R. Basco

David R. Basco  
(Member)

James R. Scoggins

James R. Scoggins  
(Head of Department)

August 1985

## ABSTRACT

Development and Validation of a Vertically  
Two-Dimensional Mesoscale Numerical Model. (August 1985)

Michael Kent Walters, B.S., Texas A&M University  
Chairman of Advisory Committee: Dr. Dusan Djuric

A vertical, two dimensional, grid-point mesoscale model is developed, using the equations of motion and thermodynamics in a dry flow. A non-dimensional vertical coordinate  $s$  is used. The hydrostatic assumption is made. To avoid the sensitivity of the continuity equation, several derived equations are used based on the first law of thermodynamics, the pressure tendency equation, and the top boundary condition, which was that the vertical motion was zero at the top boundary. These derived equations include the equation for prediction of density, Richardson's equation for vertical motion, and the pressure tendency at the top of the model. A simplified calculation of dry, subgrid convection is made to prevent instability. The equations are integrated using explicit finite differences with a time step of 2 minutes.

A test made with a static start and no forcing showed no change in initial variables. The kinetic energy budget for the model was calculated by modifying the initial state through differential heating. The test

showed a diffusion of kinetic energy of less than 1% per hour. A calculation of mass continuity using solid lateral boundaries showed mass continuity preserved to computer accuracy. Problems which occurred in duplicating the low-level jet calculations of Shen (1980) were solved by rederiving Richardson's equation with a top boundary condition in which the vertical gradient of vertical motion vanished at the top of the model, and by specifying a temperature gradient at the left boundary. Results were consistent with those reported by Shen. The conclusion is made that the model is formulated correctly and is capable of physically realistic results in two dimensions on a vertical plane. These results are consistent with the imposed boundary conditions.

## ACKNOWLEDGMENTS

The writer would like to acknowledge the help and support of his committee. In particular, I would like to express my appreciation to Dr. Dusan Djuric for his encouragement, suggestions, and readily available assistance in the preparation and completion of this work. I would also like to thank Dr. Kenneth Brundidge for his helpful comments and assistance in the final preparation of this thesis. In addition, appreciation is given to Dr. David Basco for his suggestions. Finally, I would like to thank Dr. James Scoggins for making the computer resources of the Texas A&M University Meteorology Department available for this study.

Sincere thanks are extended to the United States Air Force and the Air Force Institute of Technology for giving me the opportunity to conduct this research.

Appreciation is given to my parents, Mr. and Mrs. Earl O. Walters, whose encouragement and support made this possible.

## DEDICATION

This thesis is dedicated to my wife,

Sally,

whose encouragement keeps me going,

to my children,

Anne and Brian,

who give me purpose,

and to my parents,

who made this possible.

## TABLE OF CONTENTS

	Page
ABSTRACT . . . . .	iii
ACKNOWLEDGEMENTS . . . . .	v
DEDICATION . . . . .	vi
TABLE OF CONTENTS . . . . .	vii
LIST OF TABLES . . . . .	viii
LIST OF FIGURES . . . . .	ix
1. INTRODUCTION . . . . .	1
2. BACKGROUND AND STATEMENT OF PROBLEM . . . . .	3
a. Previous studies . . . . .	3
b. Statement of the problem . . . . .	4
3. THE NUMERICAL MODEL . . . . .	6
a. The coordinate system . . . . .	6
b. The basic governing equations . . . . .	7
c. The numerical grid system . . . . .	10
d. The lateral boundary conditions . . . . .	12
e. Method of solution of the equations . . . . .	13
f. The finite-difference equations . . . . .	14
4. MODEL VALIDATION . . . . .	23
a. Static test . . . . .	23
b. Testing of mass continuity . . . . .	25
c. Testing of the kinetic energy budget . . . . .	26
d. Nonlinear simulations . . . . .	29
e. Results of the simulation . . . . .	38
5. CONCLUSIONS AND RECOMMENDATIONS . . . . .	56
REFERENCES . . . . .	59
APPENDIX . . . . .	62
VITA . . . . .	66

## LIST OF TABLES

Table	Page
1 Initial values of model variables for static test and kinetic energy calculations . . . . .	25
2 Results of kinetic energy budget calculations . .	29
3 Surface heating rate ( $K s^{-1} \times 10^{-5}$ ) . . . . .	32
4 Initial values of variables for nonlinear simulation of low-level jet. . . . .	38

## LIST OF FIGURES

Figure		Page
1	Diagram of the vertical coordinate system. . .	6
2	Diagram of the numerical grid system . . . . .	11
3a	Isotach analysis at 4 h for v. . . . .	39
3b	Isotherms at 4 h. . . . .	39
4a	Isotach analysis at 8 h for v. . . . .	40
4b	Isotherms at 8 h. . . . .	40
5a	Isotach analysis at 12 h for v. . . . .	41
5b	Isotherms at 12 h. . . . .	41
6a	Isotach analysis at 16 h for v. . . . .	42
6b	Isotherms at 16 h. . . . .	42
7a	Isotach analysis at 20 h for v. . . . .	43
7b	Isotherms at 20 h. . . . .	43
8a	Isotach analysis at 24 h for v. . . . .	44
8b	Isotherms at 24 h. . . . .	44
9a	Isotach analysis at 28 h for v. . . . .	45
9b	Isotherms at 28 h. . . . .	45
10	Comparison of maximum speed of southerly wind 400 km from left hand boundary in Shen's model with TAMU two-dimensional model. . . . .	48
11	Vertical motion $\dot{s}$ at 28 h in $\text{cm s}^{-1}$ . . . . .	50
12	Stream function in $\text{m}^2 \text{s}^{-1}$ . . . . .	51
13	Isotach analysis at 28 h for v for no inversion case . . . . .	53
14	Time variation of the maximum southerly and easterly wind . . . . .	54

## 1. INTRODUCTION

Since the advent of computers in the 1940's it has become increasingly popular to apply them to the numerical solution of complicated fluid dynamics problems for which no analytical solutions are possible. One of the original applications of computers to the solution of such problems was in the field of meteorology. Numerical models have been developed to simulate many atmospheric processes, from land-sea breezes to global general circulation. With computer resources becoming increasingly available and powerful, many investigators have become interested in applying them to the simulation of meteorological events on horizontal scales of less than 1000 km, i.e. mesoscale events.

It has been recognized by many recent investigators that the study of the mesoscale environment is very important in understanding the growth and development of convective clouds. Ulanski and Garstang (1978) have noted that the size of the area of surface convergence is a critical factor in attempting to forecast the total amount of rainfall which can be expected to be produced by a given storm. Tripoli and Cotton (1980) pointed out that the level of kinetic energy which an individual cumulus cloud can achieve is a function of the pre-existing

The citations on the following pages follow the style of the Journal of the Atmospheric Sciences.

low-level mesoscale convergence of moist static energy. It has become increasingly evident that events on the meso $\beta$  scale, or horizontal scales of 20 km to 200 km (Orlanski, 1975), are of primary importance in the study of convective phenomena. For this reason, it is desirable to search for suitable research tools to study these phenomena.

This study was undertaken to aid in the development of a suitable numerical tool which could be used to study such important mesoscale phenomena.

## 2. BACKGROUND AND STATEMENT OF THE PROBLEM

### a. Previous studies

As part of the Texas High Plains Experiment, or HIPLEX, Djuric and Das (1982) recognized the need for a simple operational model for predicting mesoscale convergence fields of mass, moist-static energy and vorticity. They realized that such a model would be limited in scope but expected that it would prove powerful and useful in the pre-storm and early-storm conditions when the feedback from the clouds to the environment is relatively unimportant. The existing models such as the NCAR-Drexel model (Perkey, 1976), the Florida sea breeze model (Pielke, 1974; Pielke, 1976), the mesoscale models developed at Pennsylvania State University (Anthes and Warner, 1978; Warner et. al., 1978) and the NOAA/ERL models (Nickerson et. al., 1978; Nickerson et. al., 1979; Fritsch and Chappell, 1980) were deemed unsuitable for such an application because they were complex and demanded computer time which was considered excessive for a simple, real-time forecast model of the type envisioned. They also rejected the models of Tapp and White (1976), Klemp and Wilhemson (1978), Schlesinger (1978), Cotton and Tripoli (1978), and Tripoli and Cotton (1980), because they were even more complex than the previously mentioned models and were thus unsuitable for their purposes. Faced

with the alternative of adapting one of these complex models to their purpose or writing their own model, Djuric and Das (1982) chose the latter approach.

b. Statement of the problem

A three-dimensional numerical model designed to meet the requirements mentioned above was developed by Djuric and Das (1982). This model was named the TAMU Mesoscale Numerical Model. When they entered the validation phase of the model, problems began to become evident with the program itself. These difficulties were manifested as numerical instabilities which occurred unpredictably in certain grid points of their model. They traced the origin of the numerical instabilities to certain advective terms in the model, but were unable to resolve the difficulties. Because of these persistent numerical instabilities, they postponed planned modifications to their boundary conditions which they hoped would improve the model, and focused their research efforts on the removal of the numerical instabilities. However, the problem has remained unsolved.

The objective of this study is to design and verify a vertically two-dimensional mesoscale numerical model based on the equations of motion, continuity, and thermodynamics, which is capable of simulating profiles of wind and thermodynamic variables. This model will be similar

to the model of Djuric and Das (1982), except that it will be only vertically two-dimensional. Numerical testing of this vertically two-dimensional model may give insight into the nature of the numerical instabilities which plagued the TAMU model because the predictive and diagnostic equations and the finite-difference forms used in the two models will be very similar. In addition, it will be possible to test various boundary conditions which could be later used in a three-dimensional version. Successful completion of the simpler model should make possible the further systematic development of a three-dimensional version which can fulfill the requirements of Djuric and Das (1982) mentioned above.

### 3. THE NUMERICAL MODEL

#### a. The coordinate system

The model uses a terrain-following vertical coordinate system. The vertical coordinate is a non-dimensional height  $s$  with  $s = 0$  at the ground and  $s = 1$  at the top of the model, as shown in Fig. 1. The relationship between the vertical coordinate  $s$  and the height  $z$  above sea level is given by

$$s = (Z - Z_0) / (Z_t - Z_0) = (Z - Z_0) / H \quad (1)$$

where  $Z_0$  is the terrain elevation above sea level,  $Z_t$  is the height above sea level of the top of the model, and  $H$  is the model thickness in meters. The height  $Z$  at a coordinate surface  $s = \text{constant}$  is a space dependent variable, but is independent of time.

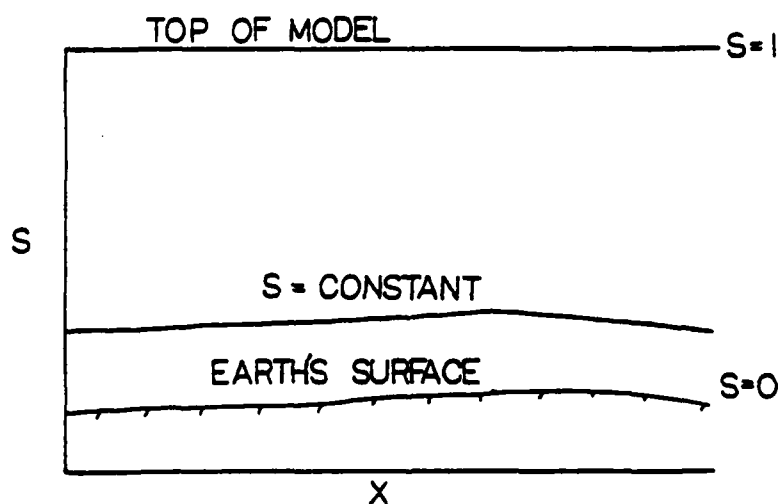


Fig. 1. Diagram of the vertical coordinate system.

b. The basic governing equations

The model uses the basic equation set used by Djuric and Das (1982) with the exception that the equation for continuity of water vapor is not used because the model is dry. The equations are as follows:

$$\frac{d\vec{V}}{dt} = -f \hat{k} \times \vec{V} - \frac{1}{\rho} \nabla p - g \nabla z + \frac{1}{\rho H^2} \frac{\partial}{\partial s} (\rho K_m \frac{\partial \vec{V}}{\partial s}) , \quad (2)$$

$$\frac{\partial p}{\partial s} = -\rho g H , \quad (3)$$

$$\frac{\partial \rho}{\partial t} + \nabla \cdot \rho \vec{V} + \frac{\partial}{\partial s} (\rho \dot{s}) + \frac{\rho}{H} \vec{V} \cdot \nabla H = 0 , \quad (4)$$

$$\frac{dT}{dt} = -\dot{s} g \frac{H}{C_p} + \frac{Q}{C_p} , \quad (5)$$

$$p = \rho R T . \quad (6)$$

The symbols to be used here are defined as follows:

$\vec{V}$  = horizontal wind vector

$\hat{k}$  = vertical unit vector

$\dot{s}$  = vertical component of wind

$x$  = horizontal coordinate

$s$  = vertical coordinate

$t$  = time coordinate

$p$  = pressure

$\rho$  = density

$f$  = Coriolis parameter

$g$  = acceleration due to gravity

$z$  = height above sea level

$H$  = thickness of the model

$K_m$  = eddy diffusivity of momentum =  $5 \text{ m}^2 \text{ s}^{-1}$

$\tau$  = eddy stress

$C_d$  = surface drag coefficient = 0.15

$T$  = temperature

$Q$  = heating rate

$C_p$  = specific heat at constant pressure

$C_v$  = specific heat at constant volume

$\gamma = C_p/C_v$

$R$  = gas constant for dry air

Equation (2) is the horizontal equation of motion, (3) is the hydrostatic equation, (4) is the continuity equation, (5) is the first law of thermodynamics, and (6) is the equation of state. Equations (2)-(6) form a complete set for dry flow when  $Q$  and  $K_m$  are specified.

To solve this equation set numerically, several derived equations are used (Djuric and Das, 1982). These are based on the pressure tendency equation

$$\frac{\partial p}{\partial t} = \left(\frac{\partial p}{\partial t}\right)_1 - g \int_s^1 \nabla \cdot (H \rho \vec{V}) ds' - g H \rho_1 \dot{s}_1 + g H \rho \dot{s} \quad , \quad (7)$$

the first law of thermodynamics, and the boundary

condition  $\dot{s} = 0$  at the top of the model. The derived equations used are the following:

$$\frac{\partial p}{\partial t} = - \vec{\nabla} \cdot \nabla p - \dot{s} \frac{\partial p}{\partial s} + \frac{p}{r_p} \left( \frac{\partial p}{\partial t} \right)_1 - \rho \left( \frac{D - \vec{\nabla} \cdot \nabla p}{\gamma p} + \frac{Q}{C_{pT}} \right) , \quad (8)$$

$$\dot{s} = - \frac{1}{r} \left( \frac{\partial p}{\partial t} \right)_1 \int_0^s \frac{ds'}{p} + \int_0^s \left[ \frac{D - \vec{\nabla} \cdot \nabla p}{\gamma p} + \frac{Q}{C_{pT}} - \frac{1}{H} \nabla \cdot H \vec{\nabla} \right] ds' , \quad (9)$$

$$\left( \frac{\partial p}{\partial t} \right)_1 = \frac{\int_0^1 \left[ \frac{D - \vec{\nabla} \cdot \nabla p}{p} + \frac{Q}{C_{pT}} - \frac{1}{H} \nabla \cdot H \vec{\nabla} \right] ds'}{\int_0^1 \frac{ds'}{p}} . \quad (10)$$

Equation (8), used for the prediction of density, is derived from the first law of thermodynamics in order to avoid the sensitivity of the continuity equation, (9) is the Richardson equation for vertical motion, and (10) is the equation for pressure tendency at the top of the model. The function  $D$  used above is the integrated divergence above the level  $s$  and is given by

$$D = g \int_s^1 \nabla \cdot (\rho H \vec{\nabla}) ds' . \quad (11)$$

The derivations of (7)-(10) are given by Djuric and Das (1982) and are presented in the Appendix.

In addition to the above derived equations, the component equations of motion are expressed in flux divergence form using (2) and (4) as follows:

$$\begin{aligned} \frac{\partial}{\partial t}(\rho u) + \frac{\partial}{\partial x}(\rho u^2) + \frac{\partial}{\partial s}(\rho u s) + \frac{\rho u^2}{H} \frac{\partial H}{\partial x} = - \frac{\partial p}{\partial x} \\ + \rho f v - \rho g \frac{\partial z}{\partial x} + \frac{1}{H} \frac{\partial}{\partial s}(\rho K_m \frac{\partial u}{\partial s}) \quad , \end{aligned} \quad (12)$$

$$\begin{aligned} \frac{\partial}{\partial t}(\rho v) + \frac{\partial}{\partial x}(\rho u v) + \frac{\partial}{\partial s}(\rho v s) = -\rho f u - \frac{\rho u v}{H} \frac{\partial H}{\partial x} \\ + \frac{1}{H} \frac{\partial}{\partial s}(\rho K_m \frac{\partial v}{\partial s}) \quad . \end{aligned} \quad (13)$$

At the lowest level of the model the internal frictional terms in (12) and (13) are replaced by  $\frac{1}{H} \frac{\partial \tau}{\partial s}$  where  $\tau$  is equal to  $\rho C_d * |u| * u$  and  $\rho C_d * |v| * v$ , respectively, at the surface, and  $C_d$  is the surface drag coefficient.

### c. The numerical grid system

The domain of integration is divided into a vertically and horizontally staggered grid similar to that used in the TAMU mesoscale model (Djuric and Das, 1982). The location of the model variables and the indices used are shown in Fig. 2. The horizontal grid points are evenly spaced at an interval of  $\Delta x/2$ , while the vertical grid points are evenly spaced at an increment of  $\Delta s/2$ .

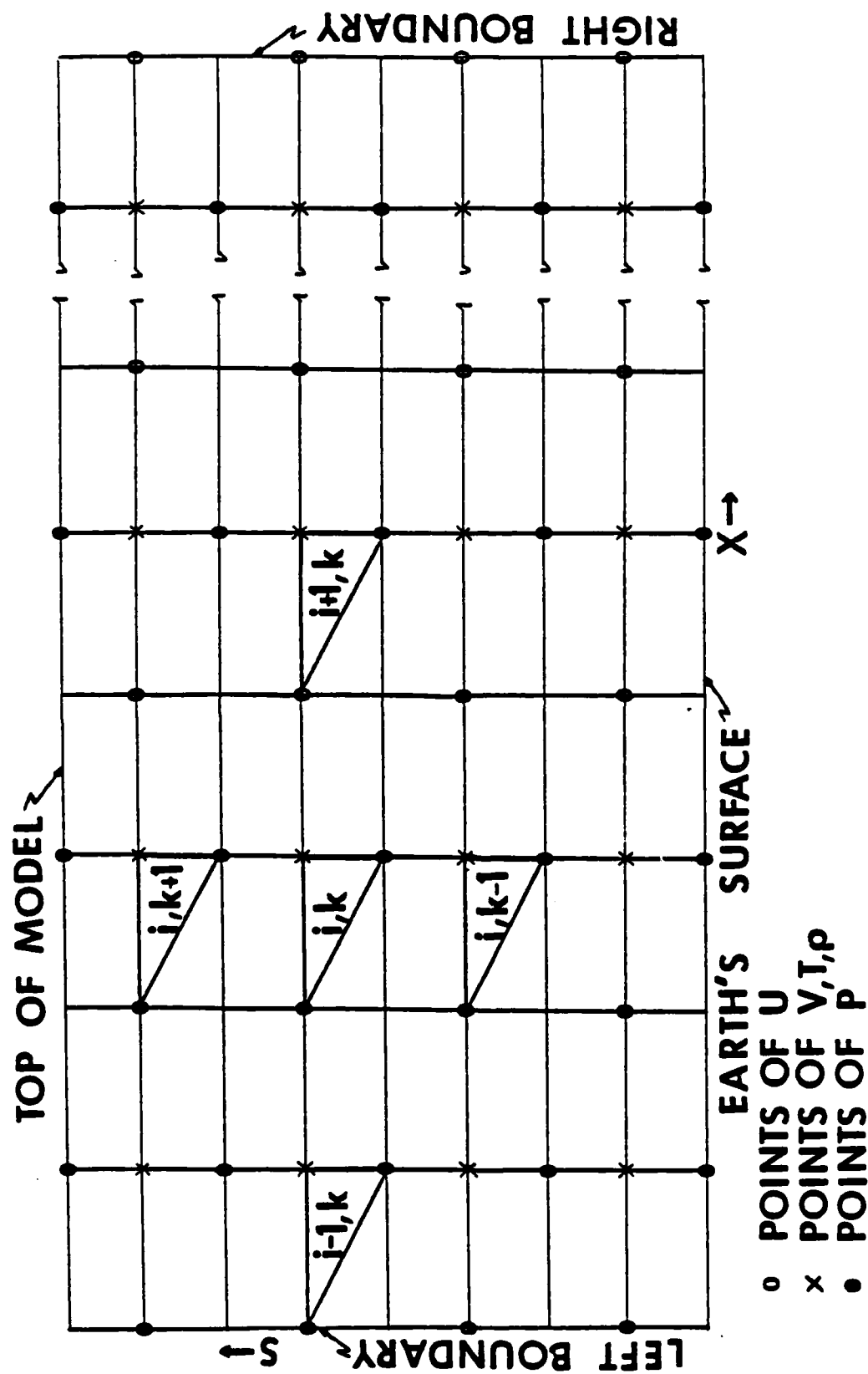


Fig. 2. Diagram of the numerical grid system.

$\Delta x$  is equal to 45 km, while  $\Delta s$  is equivalent to 250 m in the simulations to be presented here. The horizontal wind component,  $u$ , is defined on both the left and right lateral boundaries, while pressure is defined on both the upper and lower boundaries. As shown in Fig. 2., the variables are subdivided into triangular regions carrying the same computational indices, to simplify the notation.

d. The lateral boundary conditions

A simplified lateral boundary condition of  $u = 0$  is used for purposes of model validation. This boundary condition was chosen because it allows the finite difference formulas used in the interior of the model to also be applied at the lateral boundaries. Due to the centered nature of the horizontal space derivatives, use of the interior finite difference formulas at the grid points immediately adjacent to the lateral boundaries requires the knowledge of values of pressure and density outside the model. Use of this boundary condition makes it possible to set the pressure and density immediately adjacent to the boundary on the outside equal to that immediately adjacent to the boundary on the inside. This excludes the need for introducing separate forward or backward space differencing at the boundaries which would complicate the validation of the model.

e. Method of solution of the equations

Solution of the equations is accomplished in the following manner. The horizontal divergence is calculated from known wind components and densities for each level of the model. Equation (11) is then solved at each appropriate grid point. Next, the following individual parts of (10) are evaluated.

$$\frac{D - \vec{V} \cdot \nabla p}{\gamma P} \quad , \quad (14)$$

$$\frac{Q}{C_p T} \quad , \quad (15)$$

$$\frac{1}{H} (\nabla \cdot H \vec{V}) \quad , \quad \text{and} \quad (16)$$

$$\int_0^1 \frac{ds'}{p} \quad . \quad (17)$$

Once these are calculated, (14), (15), and (16) are integrated over the depth of the model. The pressure tendency at the top of the model is then found using (10), following which the Richardson equation, (9), is solved. At this point the density tendency, (8), is computed.

Next, the nonlinear components of the equations of horizontal momentum are evaluated. Once these values are known throughout, the pressure at the new time level is obtained from integration of (3) using the pressure tendency at the top of the model and the density tendency previously calculated. Temperature is then obtained diagnostically from (6) using the new values of pressure

and density. The temperature profile is checked for possible dry-convective adjustment, following which the pressure and density are recalculated hydrostatically if necessary. Finally, the u and v components of the wind are evaluated. The computation then proceeds to the next time step by repeating the entire numerical process.

f. The finite-difference equations

The preceding computational process is accomplished using the following explicit finite-difference equations, in which DX refers to the horizontal grid increment, DS refers to the vertical grid increment, variables i and k refer to spatial indicies as shown in Fig. 2, and DT is the time step. The time step used was 120 s, which was chosen to satisfy the Courant-Friedrichs-Levy (CFL) condition for computational stability. To satisfy the CFL condition DT must satisfy  $c \frac{DT}{DX} \leq 1$ , where c is the wave speed of the fastest wave expected in the model, which in this case is a sound wave with c equal to 340 m s<sup>-1</sup>, which was based on the warmest temperature expected in the model. Superscript variables n and n+1 refer to the present and future values respectively. Other superscripts refer to exponentiation in the usual manner. Subscript 1 indicates the variable is defined at the top of the model. The remaining variables have been previously defined.

The finite difference equations are as follows:

$$\nabla \cdot H \rho \vec{\nabla} (i,k) = H(i+1) * (\rho(i+1,k) + \rho(i,k)) * u(i+1,k) - H(i) * (\rho(i,k) + \rho(i-1,k)) * u(i,k) / (2 * DX) = DV(i,k), \quad (18)$$

$$g \int_0^1 (\nabla \cdot H \rho \vec{\nabla}) ds' (i,k) = \sum_{n=k}^{n=12} DS * G * DV(i,n) = DIV(i,k), \quad (19)$$

$$\vec{\nabla} \cdot \nabla p(i,k) = \nabla \cdot p \vec{\nabla} (i,k) - p \nabla \cdot \vec{\nabla} (i,k) = ((p(i,k) + p(i,k+1) + p(i+1,k+1) + p(i+1,k)) * u(i+1,k) - (p(i,k) + p(i,k+1) + p(i-1,k+1) + p(i-1,k)) * u(i,k)) / (2 DX) - (p(i,k) + p(i,k+1)) * (u(i+1,k) - u(i,k)) / DX = VDP(i,k), \quad (20)$$

$$DIV - \vec{\nabla} \cdot \nabla p / \gamma p(i,k) = (DIV(i,k) + DIV(i,k+1) - VDP(i,k)) / (1.4 * (p(i,k) + p(i,k+1))) = DVP(i,k), \quad (21)$$

$$\frac{Q}{C_p T}(i,k) = Q(i,k) / (C_p T(i,k)) = QCT(i,k), \quad (22)$$

$$\frac{1}{H} \nabla \cdot \vec{\nabla} H(i,k) = (H(i+1) * u(i+1,k) - H(i) * u(i,k)) / HP(i) = DHV(i,k), \quad (23)$$

$$\int_0^S ((D - \vec{\nabla} \cdot \nabla P / \gamma P) + QCT - DHV) ds' (i,k) = \sum_{n=2}^{n=k} DS * (DVP(i,n-1) + QCT(i,n-1) - DHV(i,n-1)) = DIS(i,k), \quad (24)$$

$$\int_0^s ds' / P(i, k) = DSP(i, k) = \sum_{n=0}^{n=k} 2DS / (p(i, n) + p(i, n-1)) , \quad (25)$$

$$\left(\frac{\partial p}{\partial t}\right)_1 = 1.4 * DIS(i, kel) / DSP(i, kel) , \quad (26)$$

$$\dot{s}(i, k) = SD(i, k) = DIS(i, k) - DIS(i, kel) * DSP(i, k) / DSP(i, kel) , \quad (27)$$

$$\begin{aligned} \left(\frac{\partial p}{\partial t}\right)(i, k) = & -\rho(i, k) * ( -DIS(i, kel) / ( DSP(i, kel) * \\ & (p(i, k+1) + p(i, k)) * 0.5 ) + (DVP(i, k) + QCT(i, k)) \\ & - ((SD(i, k+1) * (\rho(i, k+1) - \rho(i, k)) + SD(i, k) * \\ & (\rho(i, k) - \rho(i, k-1)) / 2 DS + (u(i+1, k) * (\rho(i+1, k) - \\ & \rho(i, k)) + u(i, k) * (\rho(i, k) - \rho(i-1, k)) / ( 2 * DX ) . \end{aligned} \quad (28)$$

The new u and v components of the wind are computed using a finite difference scheme which uses pressure at the new time level and trapezoidal Coriolis terms, which are averaged between the old and the new time levels. Although the use of u and v at the new time level seemingly makes the scheme implicit, it is possible to solve for u and v explicitly using the following set of equations.

$$u^{n+1} = ( AU + a * AV ) / [ \rho^{n+1} * ( 1 + a^2 ) ] ; \quad (29)$$

$$v^{n+1} = ( AV - a * AU ) / [ \rho^{n+1} * ( 1 + a^2 ) ] . \quad (30)$$

In these expressions AU, AV, and a are given by the following:

$$\begin{aligned}
 AU = & \left( -\frac{\partial p}{\partial x} \right)^{n+1} * DT + \rho^n * (u^n + a * (v^n(i) + \\
 & v^n(i-1)) / 2) - \left( \frac{1}{H^2} \frac{\partial}{\partial s} \rho K_m \frac{\partial u}{\partial s} - \frac{\partial}{\partial x} (\rho u^2)^n - \frac{\partial}{\partial s} (\rho u s)^n - \right. \\
 & \left. \left( \frac{\rho u^2}{H} \frac{\partial H}{\partial x} \right)^n \right) * DT, \quad (31)
 \end{aligned}$$

$$\begin{aligned}
 AV = & \left( -\frac{\partial}{\partial x} (\rho u v)^n - \frac{\partial}{\partial s} (\rho v s)^n - (\rho u v / H) \frac{\partial}{\partial x} \right)^n * \\
 & DT + \rho^n * (v^n - a * (u^n(i) + u^n(i+1)) / 2) \\
 & - \left( \frac{1}{H^2} \frac{\partial}{\partial s} \rho K_m \frac{\partial v}{\partial s} \right) * DT, \quad (32)
 \end{aligned}$$

and

$$a = f * DT / 2. \quad (33)$$

The internal friction terms in (31) and (32) are evaluated by the following finite difference formulas at all levels above the first level.

$$\begin{aligned}
 \frac{1}{H^2} \frac{\partial}{\partial s} \rho K_m \frac{\partial u}{\partial s} = & (K_m(i,k) * (u(i,k+1) - u(i,k)) - \\
 & K_m(i,k) * (u(i,k) - u(i,k-1))) / (DS^2 * H^2), \quad (34)
 \end{aligned}$$

$$\begin{aligned}
 \frac{1}{H} \frac{\partial}{\partial s} \rho K_m \frac{\partial v}{\partial s} = & (K_m(i,k) * (v(i,k+1) - v(i,k)) - \\
 & K_m(i,k) * (v(i,k) - v(i,k-1))) / (DS^2 * H^2). \quad (35)
 \end{aligned}$$

Boundary shear stress at the lowest level is calculated from the following:

$$\begin{aligned}
 \frac{1}{H} \frac{\partial \tau}{\partial s} = & K_m(i,k) * (u(i,2) - u(i,1)) / DS^2 - Cd * \\
 & u(i,1) * u(i,1) / DS, \quad (36)
 \end{aligned}$$

$$\begin{aligned}
 \frac{1}{H} \frac{\partial \tau}{\partial s} = & K_m(i,k) * (v(i,1) - v(i,1)) / DS^2 - Cd * \\
 & v(i,1) * v(i,1) / DS. \quad (37)
 \end{aligned}$$

Eqs. (36) and (37) assume that the eddy stress  $\tau$  is given by  $\frac{1}{H}\rho K_m \frac{\partial u}{\partial s}$  and  $\frac{1}{H}\rho K_m \frac{\partial v}{\partial s}$  in the layer immediately above the lowest layer, while the eddy stress for the lowest layer is given by  $\rho C_d * u * |u|$  and  $\rho C_d * v * |v|$ .  $K_m$  is multiplied by the initial density at the beginning of the simulation rather than the updated density at each future time step. Similarly, the Coriolis parameter and the surface drag coefficient, which are assumed constant, are multiplied by the initial value of density at each grid point prior to the first forecast step. The initial density is used because the change in density during the simulation is small, and  $f$ ,  $K_m$  and  $C_d$  are arbitrary constants. Use of the initial density for these operations takes less computation time, and introduces small error since the constants are arbitrary.

The nonlinear terms in the above formulas are evaluated according to the following finite difference formulas:

$$\frac{\partial}{\partial x} (\rho u^2)(i,k) = ( \rho(i,k) * ( u(i,k) + u(i+1,k) )^2 - \rho(i-1,k) * ( u(i,k) + u(i-1,k) )^2 ) / ( 4 * DX ) ; \quad (38)$$

$$\begin{aligned} \frac{\partial}{\partial x} (\rho u s)(i,k) = & ( ( \rho(i,k) + \rho(i,k+1) + \rho(i-1,k+1) + \\ & \rho(i-1,k) ) * ( u(i,k) + u(i,k+1) ) * ( SD(i,k+1) + \\ & SD(i-1,k+1) ) - ( \rho(i,k) + \rho(i-1,k) + \rho(i-1,k-1) + \\ & \rho(i,k-1) * ( u(i,k) + u(i,k-1) ) * ( SD(i,k) + \\ & SD(i-1,k) ) ) ) / ( 16 * DS ) ; \quad (39) \end{aligned}$$

$$\frac{1}{H} \rho u^2 \frac{\partial H}{\partial x} (i,k) = ( (\rho(i,k) + \rho(i-1,k)) * (u(i,k))^2 * (HP(i) - HP(i-1)) / (H(i) * DX) ) ;$$

(40)

$$\frac{\partial}{\partial x} \rho u v (i,k) = ( (\rho(i,k) + \rho(i+1,k)) * u(i+1,k) * (v(i,k) + v(i+1,k)) - (\rho(i,k) + \rho(i-1,k)) * u(i,k) * (v(i,k) + v(i-1,k)) ) / (4 * DX) ;$$

(41)

$$\frac{\partial}{\partial s} \rho v s (i,k) = ( (\rho(i,k) + \rho(i,k+1)) * SD(i,k+1) * (v(i,k) + v(i,k+1)) - (\rho(i,k) + \rho(i,k-1)) * SD(i,k) * (v(i,k) + v(i,k-1)) ) / (4 * DS) ;$$

(42)

$$\frac{1}{H} \rho u v \frac{\partial H}{\partial x} (i,k) = \rho(i,k) * (u(i,k) + u(i+1,k)) * v(i,k) * (H(i+1) - H(i)) / (2 * H * DX) .$$

(43)

The remaining variables to be forecast are pressure and density. Density at the new time level is computed after (28) is solved by the following:

$$\rho^{n+1} (i,k) = \rho^n (i,k) + DT * \frac{\partial \rho}{\partial t} (i,k) .$$

(44)

In (44), the superscript n+1 refers to the forecast time level and the superscript n refers to the present time level. After the pressure tendency at the top of the model is calculated from Eq. (26), the pressure at the top can be computed by the following:

$$p(i,kel) = p(i,kel) + DT * \left(\frac{\partial p}{\partial t}\right)_1 . \quad (45)$$

In the above finite difference formulas the vertical index kel refers to the top of the model. At this point it is possible to compute the pressure at remaining points using the hydrostatic equation in the following finite difference form:

$$p(i,k) = p(i,k+1) + g * DS * (HP(i)) * \rho(i,k) . \quad (46)$$

In the above finite difference formulas, H refers to the thickness of the model at columns where u is defined, and HP refers to the model thickness at columns where pressure, density, v and T and defined, as shown in Fig. 2.

Because the equation set used is hydrostatic and ignores any buoyancy contribution to vertical motion, a dry convective adjustment is made similar to that described by Haltiner and Williams (1980). At each time step the vertical profile of temperature is examined for superadiabatic lapse rates in each layer. If the lapse rate is found to be superadiabatic in any layer, it is adjusted to a slightly subadiabatic lapse rate by correcting the temperature at the top and bottom of the layer. This process simulates subgrid scale dry convection in which convection transports heat vertically

until a neutral lapse rate is established. The kinetic energy of the convective transport is assumed to be dissipated into heat energy. The correction process is iterative in that after a correction is made at one layer, the adjacent layers are reexamined. The process is repeated until no segment of the temperature profile is superadiabatic. Because this correction is made at each time step, the resultant temperature change in each layer is small. The formula used for the dry-convective adjustment is as follows:

$$T^{1'} = T^1 + \Delta t \quad ; \quad T^{0'} = T^0 - \Delta t \quad , \quad \text{where}$$

$$\Delta t = ( (T^0 - T^1) - 0.0096 * DS * H ) / 2 \quad . \quad (47)$$

and  $T^1$  and  $T^0$  are the temperature at the top and the bottom of the layer to be adjusted, respectively. This equation approximates the potential energy conserving form given by Haltiner and Williams (1980), and requires much less calculation time. Eq. (47) differs from the form given by Haltiner and Williams (1980) in that the lapse rate is slightly subadiabatic after the adjustment rather than adiabatic. Because the model is hydrostatic, total potential energy is conserved during the convective adjustment process if the mean temperature of each layer is conserved during the adjustment (Haltiner and Williams, 1980).

The x component of the wind is smoothed horizontally at each time step using a simple three point operator as follows:

$$u(i) = 0.90 u(i) + 0.05 ( u(i-1) + u(i+1) ) . \quad (48)$$

This horizontal smoothing is used to prevent spurious growth of short waves in the model. The short waves which result in the model simulations when smoothing by (48) is not performed result from grid noise due to the spatial averaging in the finite-difference equations. These short waves are minor and do not contribute to instability in the model, however, they are unrealistic meteorologically and are removed from the final result for esthetic reasons.

#### 4. MODEL VALIDATION

Before a numerical model can be used, it is necessary to perform basic validation tests to establish the credibility of the model and insure that no errors have been made in programming the model equations. These tests provide an important means of debugging the numerical scheme. The validation tests performed on the mesoscale model consisted of a simple static test, calculation of the mass continuity and the kinetic energy budget, and performing non-linear simulations which yield physically expected results which can be compared with the results of previous models.

##### a. Static test

The most basic type of test which a numerical scheme must pass is a static test, in which an equilibrium initial condition is allowed to remain at rest without any forcing applied. This test checks that all of the terms which should be zero in the numerical scheme are coded correctly and are in fact making no contribution to the result. Such a static test was performed with a domain size of 30 horizontal grid points and 13 vertical grid points, with a horizontal grid interval of 45 km and a vertical grid spacing of 250 m. The initial state was constructed so that the horizontal derivatives of all

variables were nonexistent initially, with initial wind of zero at all grid points. The initial pressure was calculated hydrostatically by specifying the surface temperature, the temperature lapse rate, and the pressure at the top of the model. Once the pressure is calculated at all points the density is computed using the equation of state. The initial values of all variables for the static test are presented in Table 1. The temperature lapse rate was specified at  $8 \text{ K km}^{-1}$ . As can be noted, this initial distribution of variables assumes a flat model, with no terrain. From this initial starting condition the model was run for 36 h with no change in the initial state. An additional test run was made in which the bottom of the model sloped so that the value of  $H$  at the left boundary was 1 km, while the top remained at 3 km. The initial variables were determined in the same manner as the previous test, with the surface temperature adjusted to fit the lapse rate specified as the surface sloped upward in the model. Variables at the right boundary were the same as given in Table 1. Because the surfaces in this case sloped, the horizontal ( $s$ ) derivatives no longer vanished, except at the top of the model. All pressure surfaces were horizontal with respect to sea level. This test also showed no change in the initial state due to the inclusion of the terms involving the geometry of the coordinate system. For all further

testing, the model was assumed to be flat.

Table 1. Initial values of model variables for static test and kinetic energy calculations.

Height (m)	T (K)	P (mb)	Density (kg/m <sup>3</sup> )
3000		690.0	
2875	267.0		0.915
2750		712.0	
2625	269.0		0.938
2500		735.0	
2375	271.0		0.960
2250		759.0	
2125	273.0		0.984
2000		783.0	
1875	275.0		1.010
1750		808.0	
1625	277.0		1.030
1500		833.0	
1375	279.0		1.060
1250		859.0	
1125	281.0		1.080
1000		885.0	
875	283.0		1.110
750		912.0	
625	285.0		1.130
500		940.0	
375	287.0		1.160
250		969.0	
125	289.0		1.190
0		998.0	

b. Testing of mass continuity

The boundary conditions used are a severe test for the mass budget of the model because no flux of any quantity occurs at the model boundaries. To check the conservation of mass in the model, an approximation of the total mass initially was made by summing the values of the density over all interior grid points where density is

defined. The calculation was repeated at the end of the simulation. This procedure was carried out during the kinetic energy budget calculations to be discussed in the next section. The result after 36 h showed a net increase of the total density of 0.0004%. This small increase is negligible and can be attributed to truncation errors in the finite-difference approximations and computer round off error. The accuracy of the computer on which the model was run is limited to six digits in single precision, which is sufficient to explain this small density variation. These results indicate that the mass continuity of the model is satisfied, with no spurious destruction or generation of mass occurring due to programming error or the finite-difference equations used.

### c. Testing of the kinetic energy budget

This test followed the general procedure of the kinetic energy testing described by Pielke (1981). Using the flux-divergence form of the equations of motion, (12) and (13), together with the horizontal components of (2), the following kinetic energy equation can be derived.

$$\begin{aligned} \frac{\partial}{\partial t} K = & -\frac{1}{2} \frac{\partial}{\partial x} \rho u v^2 - \frac{1}{2} \frac{\partial}{\partial x} \rho u^3 - \frac{1}{2} \frac{\partial}{\partial s} \rho v^2 \dot{s} - \frac{1}{2} \frac{\partial}{\partial s} \rho u^2 \dot{s} - \\ & u \frac{\partial p}{\partial x} + \rho v F_2 - \frac{1}{2} \frac{\rho u v^2}{H} \frac{\partial H}{\partial x} - \rho u g \frac{\partial z}{\partial x} + \rho u F_1 - \frac{1}{2} \frac{\rho u^3}{H} \frac{\partial H}{\partial x} . \quad (49) \end{aligned}$$

In this equation  $K$  is equal to  $\rho(u^2+v^2)/2$ . It should be noted that this kinetic energy equation neglects the contribution of  $\dot{s}$  to the kinetic energy because it is negligible compared to the horizontal motions. The equation is an expression of the kinetic energy change per unit volume since density is used in the expression for kinetic energy rather than mass. By calculating the individual terms of this equation and integrating over the domain of the model, an estimate of the expected kinetic energy change for the entire model can be made. The individual terms in (49) are calculated using finite-difference formulas which are similar to those used in the model forecast. The finite-difference formulas used in this calculation are centered on grid points where the  $x$  component of the wind is defined. Performing this calculation at each time step allows an estimate of the rate of change of total kinetic energy per unit volume for the model from which the total kinetic energy per unit volume at the next time step can be obtained. This is compared periodically with the observed kinetic energy, which is calculated from the observed winds and density, also centered on grid points where  $u$  is defined so that the two quantities can be compared. According to Pielke (1981), if the two results closely agree, the modeler can be certain that mistakes, such as coding errors, are not causing significant sources of unexplained changes of

kinetic energy. To perform this calculation a model domain of 40 horizontal grid points and 13 vertical grid points was forced by slowly heating the left hand side of the model at two grid columns. The heating rate was sufficient to cause a temperature change of  $0.35 \text{ K h}^{-1}$  at the left hand boundary.

The results of this test are given in Table 2. They indicate that the rate of kinetic energy increase calculated by the model is about  $1\% \text{ h}^{-1}$  less than that calculated by the individual terms on the right hand side of (46). According to Anthes and Warner (1978), the difference between the two different calculations is partly due to truncation errors in the horizontal and vertical flux terms in the equation of motion. The remainder of the difference can be attributed to numerical diffusion which results from the finite-difference scheme used in the forecast. Based on these results, the conclusion is made that no programming errors are contributing to spurious generation of kinetic energy in the model domain, although some damping of kinetic energy does occur. The initial conditions for this test were the same as those given in Table 1., except for the warming of the left side of the model.

Table 2. Results of kinetic energy budget calculations. Column A gives the total integrated kinetic energy per unit volume as observed from the model forecast. Column B gives the total calculated from individual terms in Eq. 49.

Hours	A ( J m <sup>-3</sup> )	B ( J m <sup>-3</sup> )
1	0.845	0.831
2	2.94	2.96
3	5.33	5.43
4	8.00	8.23
5	11.00	11.40
6	14.2	14.8
7	17.6	18.6
8	21.2	22.6
9	24.9	26.8
10	28.6	31.1
11	32.4	35.5
12	36.1	40.0
13	40.0	44.8
14	43.9	49.8
15	48.0	55.0
16	52.4	60.7
17	57.1	66.7

d. Nonlinear simulations

In addition to the basic tests described above, an attempt was made to duplicate the model results obtained by Shen (1980) in his simulation of the development of a low-level jet. Successful comparison of such a simulation with the work of Shen (1980) will give further support to the validity of this numerical scheme. In order to successfully carry out this simulation, changes in the boundary conditions of the model were made as described below. Because Shen's model did not include any terrain,

the simulation here was performed with a flat model so that the results could be compared more directly.

1) Boundary conditions

In order to duplicate the work by Shen (1980), it was necessary to change the boundary conditions from those used in the first portion of numerical testing. While the boundary conditions used above have certain advantages for numerical testing of the interior finite-difference formulas, they are inappropriate for a realistic simulation of a low-level jet similar to that carried out by Shen (1980).

For this purpose the top boundary condition was chosen to be  $\frac{\partial \dot{s}}{\partial s} = 0$  and  $\frac{\partial p}{\partial t} = 0$ . These are identical to the boundary conditions used by Shen (1980). The pressure tendency at the top of the model was set equal to zero in order to isolate the problem from the effects of levels higher than 3 km. The flux through the top of the model allows for the expected subsidence or downward vertical motion to occur when the model is forced at the left boundary. The top boundary condition used in the earlier part of the testing,  $\dot{s} = 0$ , was also tried for this portion of the simulation, but caused significant return flow at the upper levels on the left hand boundary, which is inconsistent with the forcing applied at this boundary and thus considered somewhat unrealistic. This boundary

condition is best used when the top boundary is far removed from the computational region of interest, which is not the case for this simulation. For this reason, and in order to provide better comparison with the work of Shen (1980), the top boundary conditions were changed as described. In addition, the left boundary was moved to a column where  $p$  was defined, rather than a column of  $u$  as shown in Fig. 2. The  $x$  and  $y$  components of the wind were calculated next to the left boundary by a simple forward differencing of (12) and (13) because the finite-difference scheme used for the interior points could not be used here. At the left boundary the boundary condition applied was

$$\frac{\partial T}{\partial x} = -4.44 \times 10^{-5} \left(1 - \frac{k}{12}\right) \text{ K m}^{-1}, \quad (50)$$

where  $k$  is the vertical index. This provides a temperature difference at the left hand boundary of 2 K across the grid interval nearest to the left boundary. This temperature gradient decreases to zero at the top of the model. This is consistent with an assumption of warming occurring outside the model domain which causes the left boundary to be slightly warmer than the nearest grid point in the interior. This warming at the boundary was also specified in the interior portions of the model in a manner which decreased it exponentially to zero

farther from the left boundary in the positive  $x$  direction. This was accomplished by assuming an exponential profile of  $Q$  in the  $x$  direction, with a maximum value at the left end of the model, decreasing to zero in the  $x$  direction in the interior. This heating rate was a maximum at the ground and decreased linearly to zero at the top of the model. The surface heating rate is given in Table 3. Heating the model in this manner combined with the left boundary condition described above

Table 3. Surface heating rate (  $K s^{-1} \times 10^{-5}$  ). Values decrease linearly to zero at the top of the model.

$\Delta x$	$Q/C_p$
2	22.08
3	13.40
4	8.13
5	4.92
6	2.98
7	1.81
8	1.10
9	0.66
10	0.40
11	0.24
12	0.15
13	0.09
14	0.04
15	0.03
16	0.02
17	0.01
18	0.00

insured that the left boundary was always slightly warmer than the nearest interior grid point and thus outflow was achieved at the left boundary. This combination of

forcing mechanisms is similar to that used by Shen (1980), who specified a heating rate at the left hand boundary only. For this reason Shen's model became considerably warmer at the left hand boundary than at the nearest internal grid point, building a horizontal temperature gradient of 20 K over the first grid spacing adjacent to the left boundary over his 28 h forecast period. The forcing used here implies a strong horizontal diffusion of heat, and prevents a large temperature gradient from occurring at the left boundary as in Shen's model. The pressure gradient at the right boundary was assumed zero, following the procedure of Shen (1980). The above forcing mechanism was chosen because it is similar to that used by Shen (1980), although it is not physically realistic because no diurnal variation of the heating is allowed.

## 2) Rederivation of Richardson's equation.

Because the form of Richardson's equation used in the earlier validation testing was derived using a top boundary condition of  $\dot{s} = 0$ , it was necessary to rederive this equation. The following equation used in the derivation is presented by Djuric and Das (1982):

$$\frac{\partial \dot{s}}{\partial s} = - \frac{1}{\gamma p} \frac{dp}{dt} + \frac{Q}{C_p T} - \frac{1}{H} \nabla \cdot H \vec{V} \quad . \quad (51)$$

Applying the top boundary condition  $\frac{\partial \dot{s}}{\partial s} = 0$  and assuming  $Q = 0$  at the top of the model gives the following

relationship:

$$\left(\frac{dp}{dt}\right)_1 = - \left( \frac{\gamma p}{H} \nabla \cdot H\vec{V} \right)_1 \quad (52)$$

Also given by Djuric and Das (1982) is the following equation:

$$\frac{dp}{dt} = (\vec{V} \cdot \nabla p)_1 - g \int_s^1 \nabla \cdot H\rho\vec{V} ds' + \left(\frac{\partial p}{\partial t}\right)_1 - g\rho_1 H\dot{s}_1, \quad (53)$$

which can be written as

$$\left(\frac{dp}{dt}\right)_1 = (\vec{V} \cdot \nabla p)_1 - g\rho_1 H\dot{s}_1 + \left(\frac{\partial p}{\partial t}\right)_1 \quad (54)$$

since the integral vanishes at  $s=1$ .

Combining (52) and (54) gives the following:

$$\left(\frac{\partial p}{\partial t}\right)_1 = - \frac{\gamma p}{H} (\nabla \cdot H\vec{V})_1 - (\vec{V} \cdot \nabla p)_1 + g\rho_1 H\dot{s}_1. \quad (55)$$

Substituting (53) into (51) yields:

$$\begin{aligned} \frac{\partial \dot{s}}{\partial s} = & - \frac{1}{\gamma p} \left[ \vec{V} \cdot \nabla p - g \int_s^1 (\nabla \cdot H\rho\vec{V}) ds' - g\rho_1 H\dot{s}_1 \right. \\ & \left. + \left(\frac{\partial p}{\partial t}\right)_1 \right] + \frac{Q}{C_p T} - \frac{1}{H} \nabla \cdot H\vec{V}. \end{aligned} \quad (56)$$

Eq. (55) can be substituted into this equation to give:

$$\frac{\partial \dot{s}}{\partial s} = - \frac{1}{\gamma p} \left[ \vec{V} \cdot \nabla p - (\vec{V} \cdot \nabla p)_1 - g \int_1^s (\nabla \cdot H \rho \vec{V}) ds' - \right. \\ \left. - \frac{\gamma p_1}{H} (\nabla \cdot H \vec{V})_1 \right] + \frac{Q}{C_p T} - \frac{1}{H} \nabla \cdot H \vec{V} \quad (57)$$

which can be integrated to yield the Richardson's equation as follows:

$$\dot{s} = \frac{1}{\gamma} (\vec{V} \cdot \nabla p)_1 \int_0^s \frac{ds'}{p} + \int_0^s \left( \frac{D - \vec{V} \cdot \nabla p}{\gamma p} + \frac{Q}{C_p T} - \frac{1}{H} \nabla \cdot H \vec{V} \right) ds' \\ + \frac{p_1}{H} (\nabla \cdot H \vec{V})_1 \int_0^s \frac{ds'}{p}, \quad (58)$$

where the function D is the same as previously defined. Application of the other top boundary condition eliminates the first term in this equation. It can be noted that only one term of this form of Richardson's equation is different from the previous form. For this reason little additional programming was necessary to include the new top boundary conditions. The equation for density tendency becomes

$$\frac{\partial \rho}{\partial t} = - \vec{V} \cdot \nabla \rho - \dot{s} \frac{\partial \rho}{\partial s} + \frac{\rho}{\gamma p} \left[ \left( \frac{\partial p}{\partial t} \right)_1 - g h \rho_1 \dot{s}_1 \right] - \\ \rho \left( \frac{D - \vec{V} \cdot \nabla p}{\gamma p} + \frac{Q}{C_p T} \right). \quad (59)$$

Derivation of this equation follows that given in the Appendix, with the term involving  $\dot{s}$  at the top included.

It can be noted from (55) that  $(\frac{\partial p}{\partial t})_1 = 0$  requires the following relationship:

$$(\frac{\chi p}{H})_1 (\nabla \cdot H\vec{V})_1 = g\rho_1 H\dot{s}_1 \quad . \quad (60)$$

This equation is used to determine  $u$  at the top boundary by integrating from the right boundary where  $u$  is zero, to the left boundary. This provides a slight horizontal convergence at the top of the model to counteract the subsidence so that the resultant pressure tendency at the top of the model vanishes. This is necessary for the wind field at the top of the model to be dynamically consistent with the boundary conditions stated. Using (60) to find  $u$  at the top boundary results in a very small  $u$  field because the necessary convergence required by (60) is small. Following the integration of (60), the  $v$  field at the top is obtained using the horizontal equation of motion for  $v$ , with the assumption that the vertical advection term is small. The resultant correction of  $u$  and  $v$  at the top of the model, while dynamically consistent with the boundary conditions, actually has very little effect on the results obtained. This was shown by making an additional simulation in which the simple condition  $u = v = 0$  at the top was used, effectively ignoring the right hand of (60). While not dynamically consistent, virtually identical results were obtained. This is due to the fact that the pressure

tendency at the top is quite important, appearing in the density tendency equation at all levels, while the wind at the top of the model is used only in the vertical advection terms in the equations of motion and in the calculation of internal friction at the top of the model where a vertical derivative of the wind is required. Both the vertical advection terms and the internal friction terms involved are very small, and have little effect on the rest of the computation.

### 3) Initial conditions

The initial conditions used for the simulations consisted of a slightly stable boundary layer, capped by an inversion. Initial values for all variables are given in Table 4. The temperature lapse rate assumed in the boundary layer was  $8 \text{ K km}^{-1}$ , slightly less than dry adiabatic. The pressure surfaces were all calculated using the hydrostatic equation based on the initial temperature profile and the pressure at the top of the model. Density was calculated from the pressure and temperature using the equation of state. The initial wind field was zero throughout. The initial values of all variables were horizontally uniform, because the model was assumed to be flat.

e. Results of the simulation

The equations were integrated for 28 h beginning with the initial conditions given in Table 4. The resulting flow was forced by a combination of the left boundary condition and the heating in the interior of the model. Results are shown in the sets of Figs. 3 - 9. The first figure in each set consists of an x - s cross section showing an isotach analysis of the v component of the

Table 4. Initial values of variables for nonlinear simulation of low-level jet.

Height (m)	T (K)	P (mb)	Density (kg/m <sup>3</sup> )
3000		677.0	
2875	267.0		0.898
2750		699.0	
2625	269.0		0.920
2500		721.5	
2375	271.0		0.942
2250		744.6	
2125	273.0		0.965
2000		768.3	
1875	275.0		0.989
1750		792.5	
1625	277.0		1.012
1500		817.3	
1375	264.0		1.096
1250		844.1	
1125	266.0		1.124
1000		871.7	
875	268.0		1.151
750		899.9	
625	270.0		1.180
500		928.8	
375	272.0		1.209
250		958.4	
125	274.0		1.238
0		988.7	

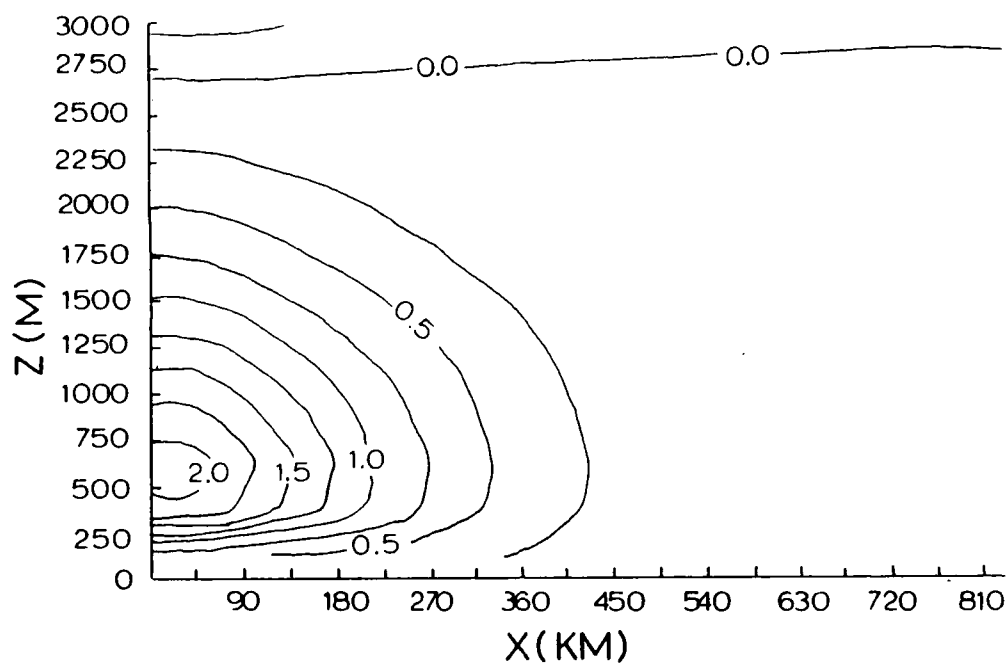


Fig. 3a. Isotach analysis at 4 h for v.

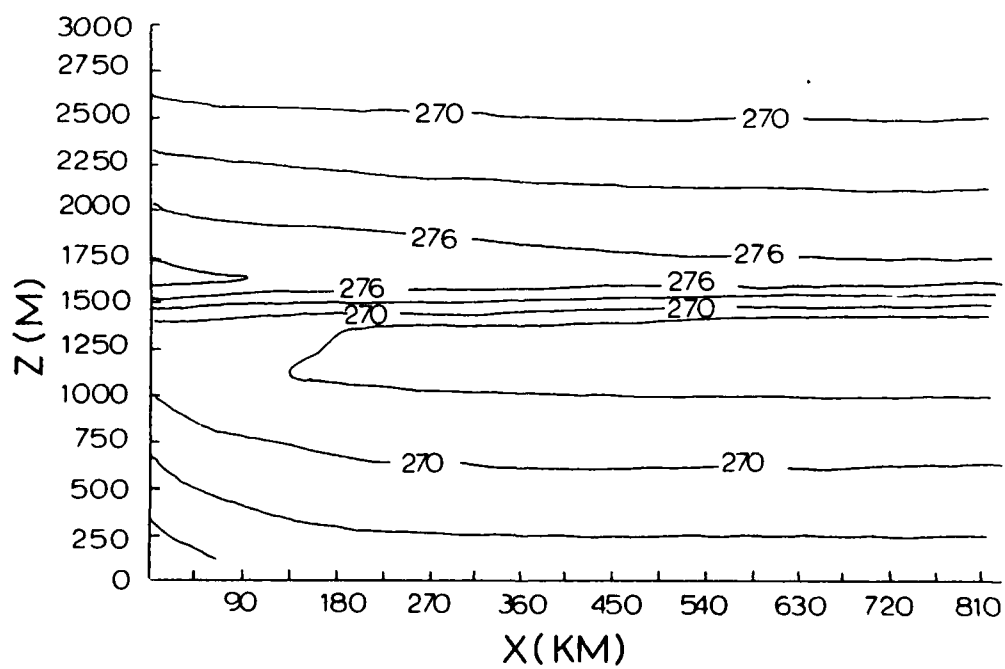


Fig. 3b. Isotherms at 4 h.

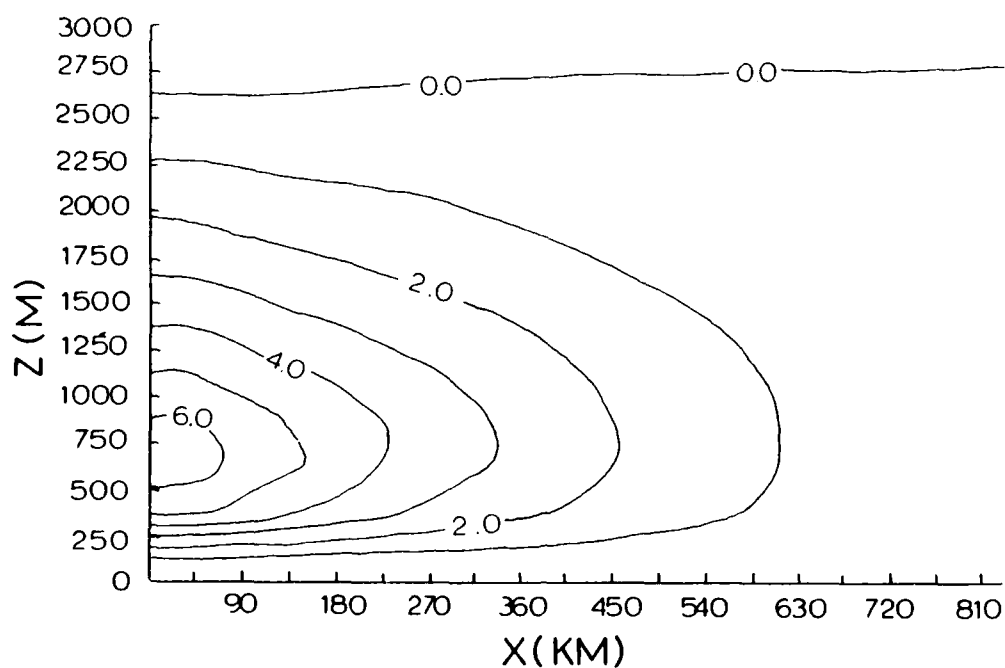


Fig. 4a. Isotach analysis at 8 h for  $v$ .

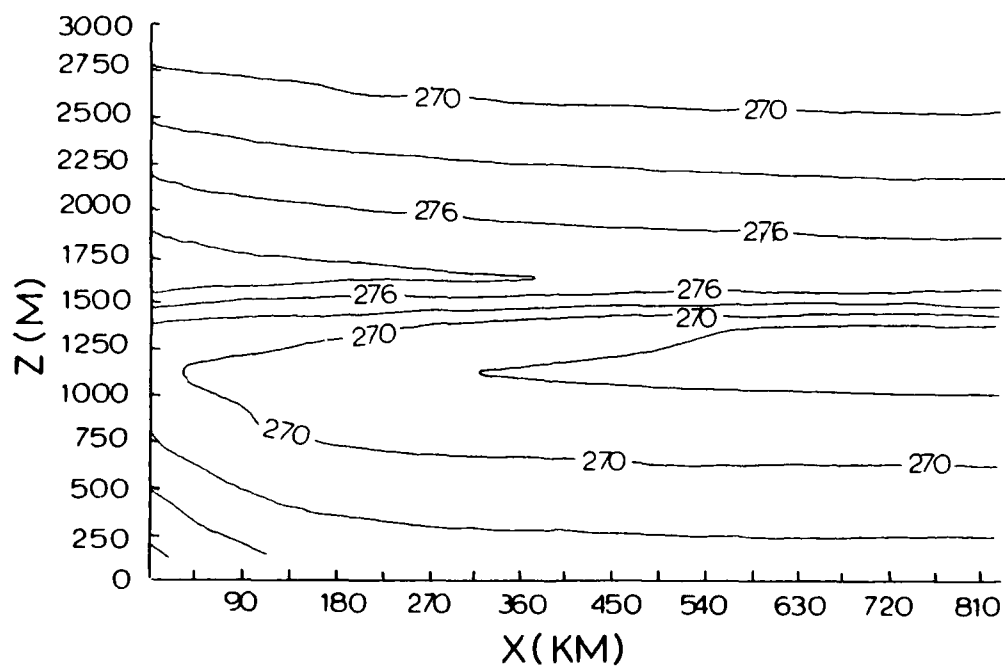


Fig. 4b. Isotherms at 8 h.

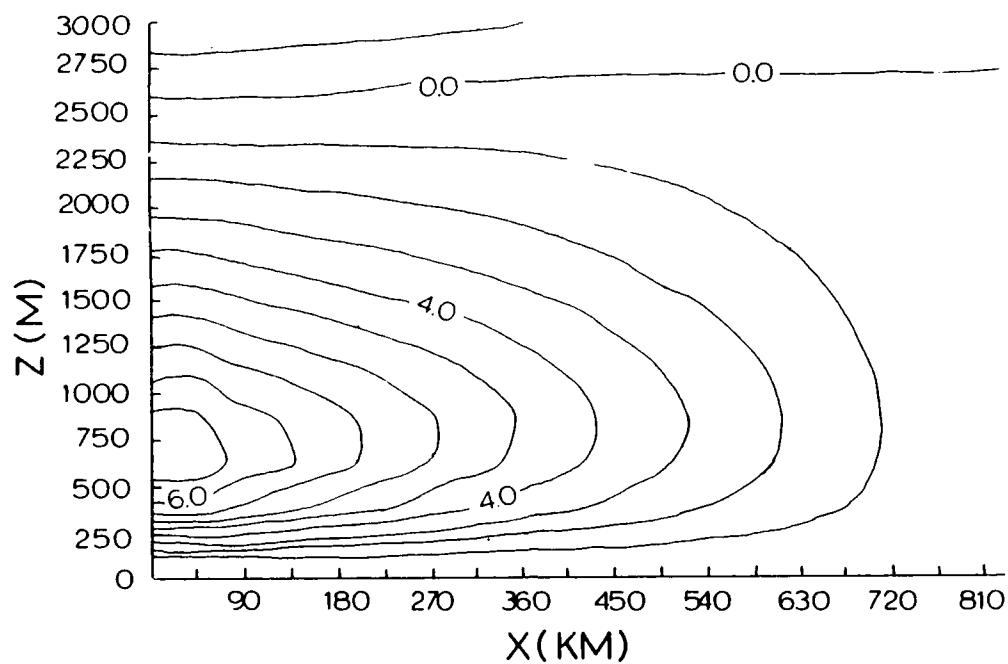


Fig. 5a. Isotach analysis at 12 h for v.

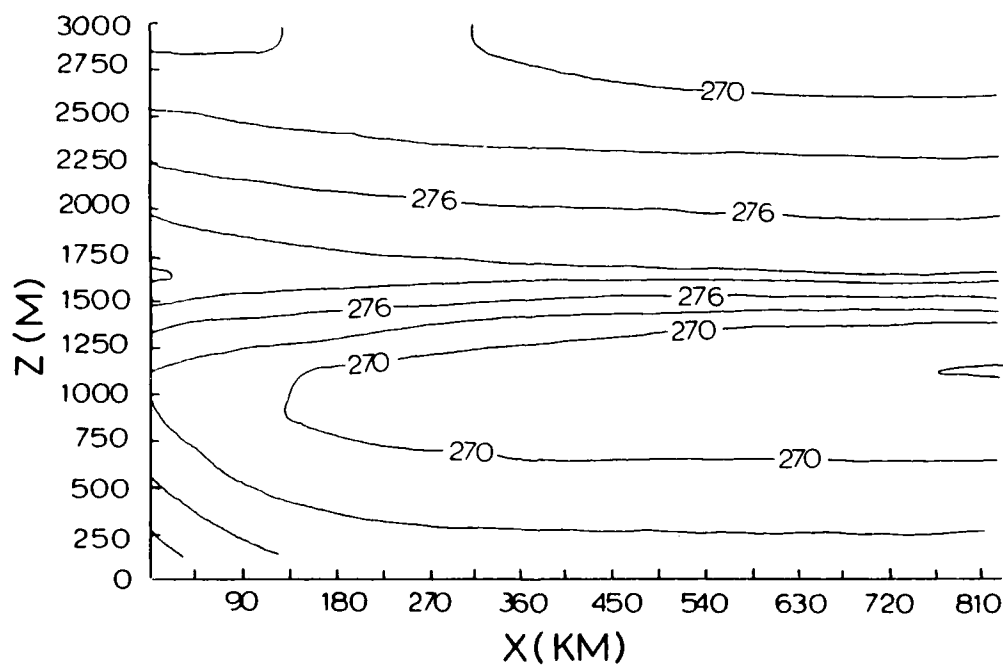


Fig. 5b. Isotherms at 12 h.

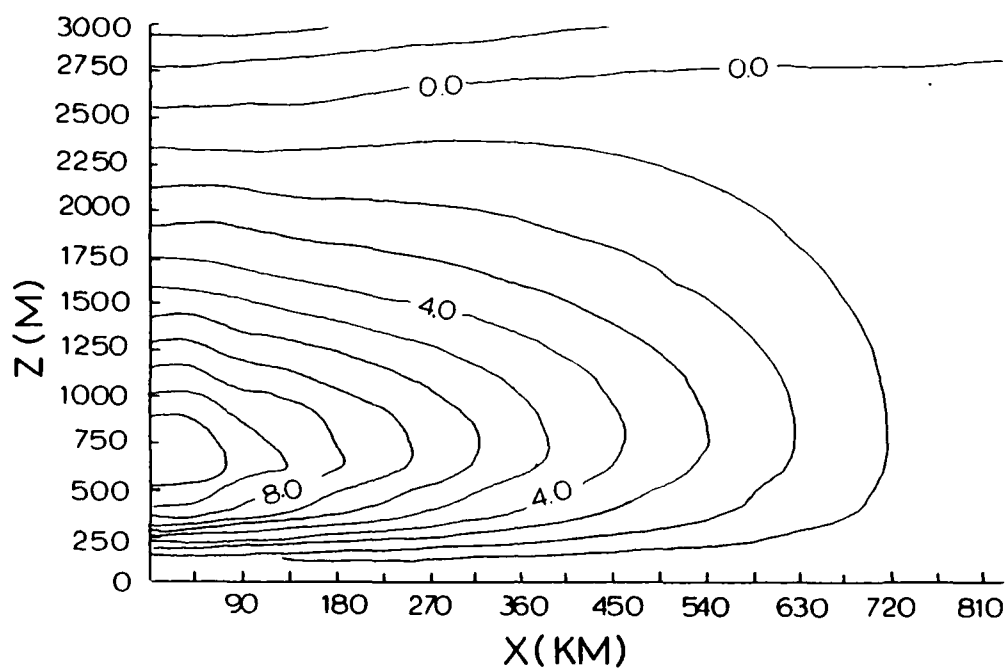


Fig. 6a. Isotach analysis at 16 h for v.

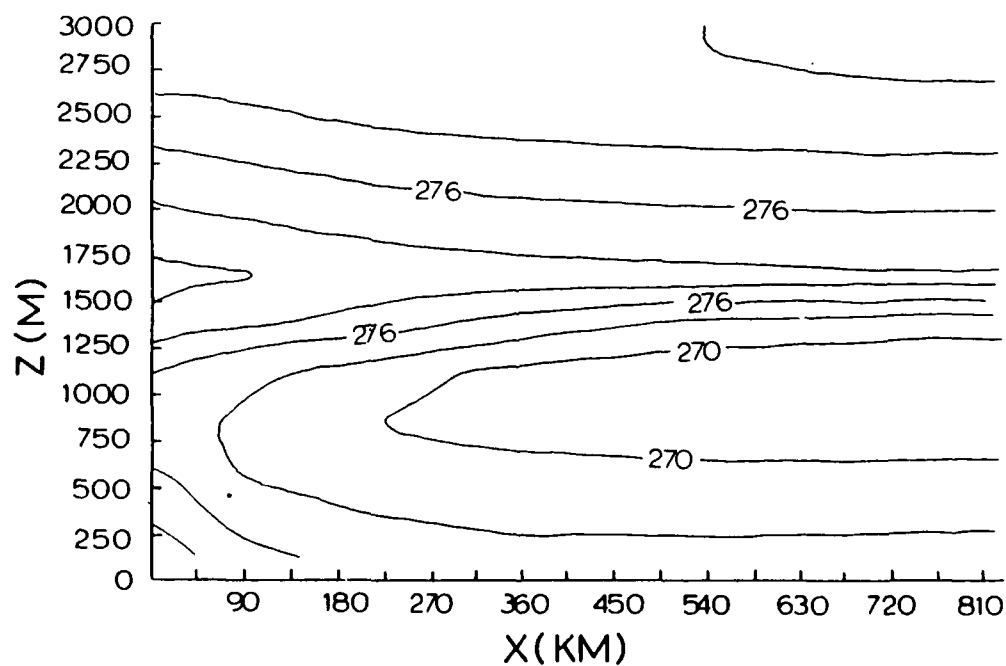


Fig. 6b. Isotherms at 16 h.

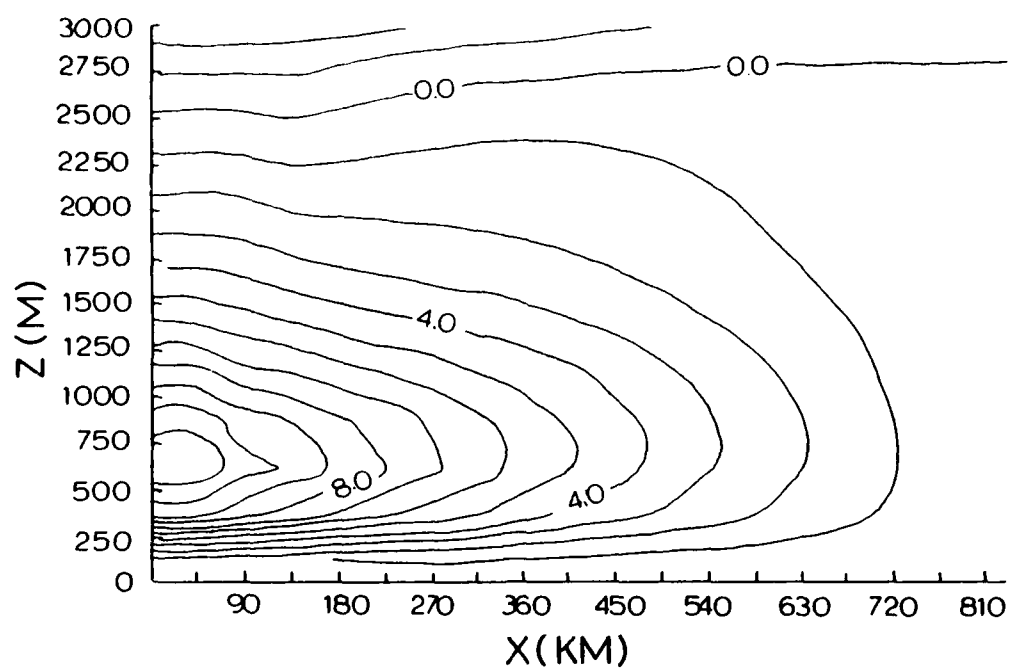


Fig. 7a. Isotach analysis at 20 h for  $v$ .

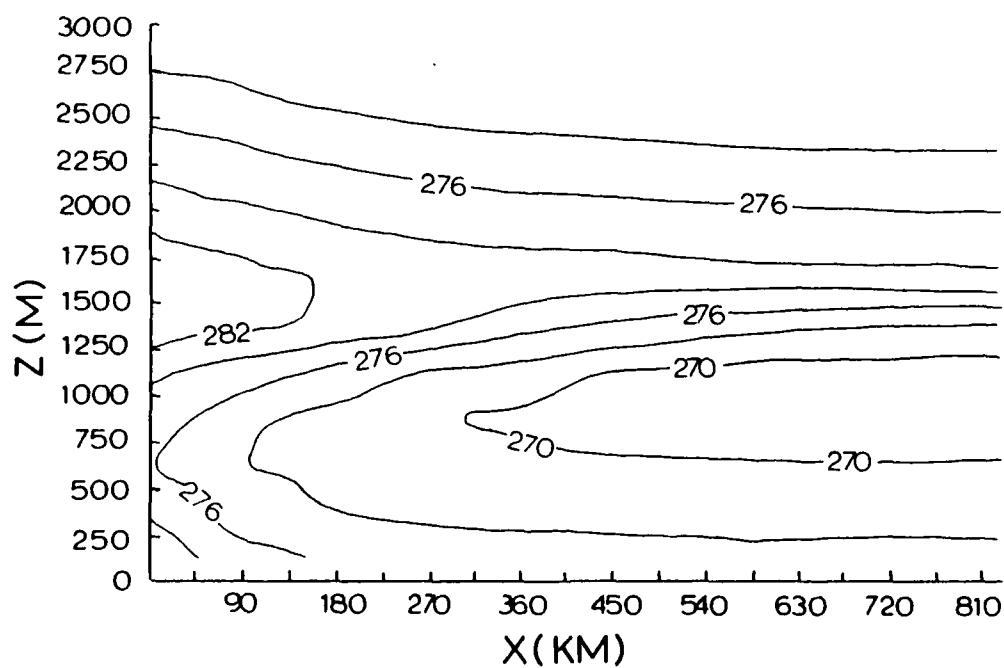


Fig. 7b. Isotherms at 20 h.

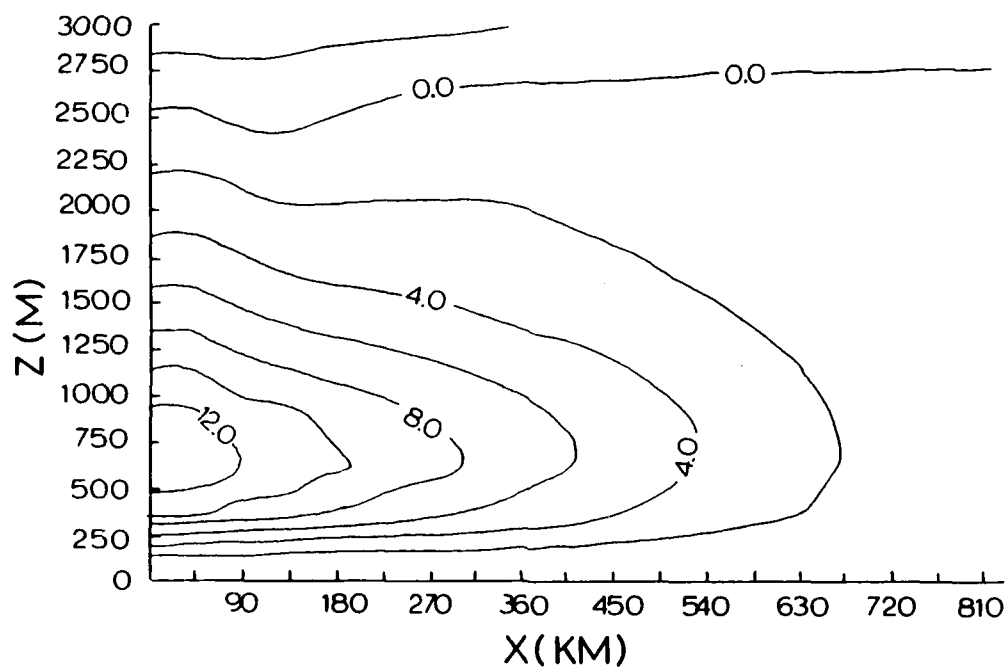


Fig. 8a. Isotach analysis at 24 h for  $v$ .

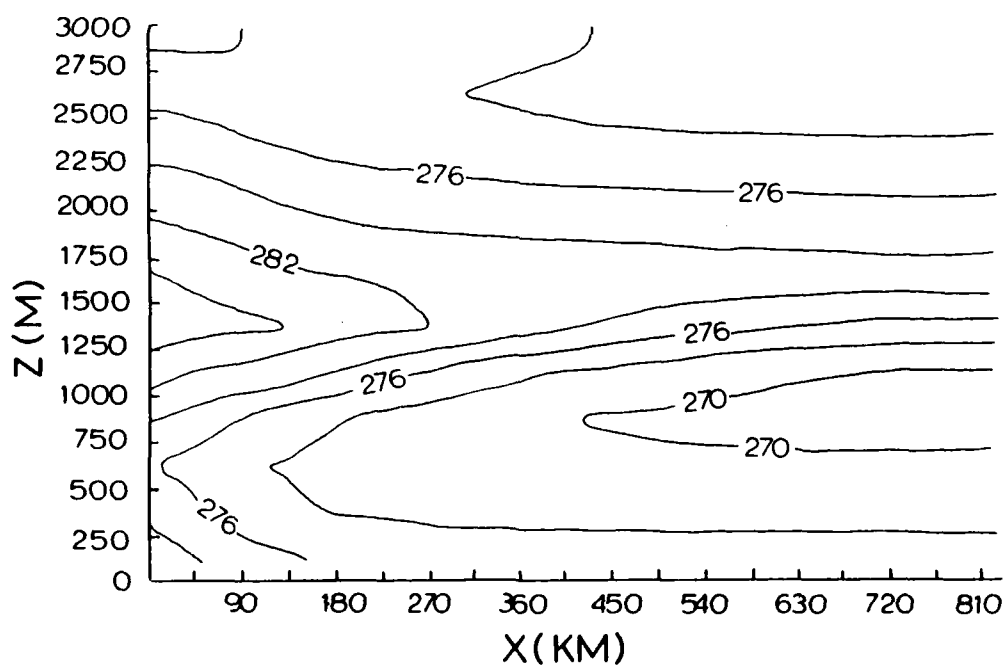


Fig. 8b. Isotherms at 24 h.

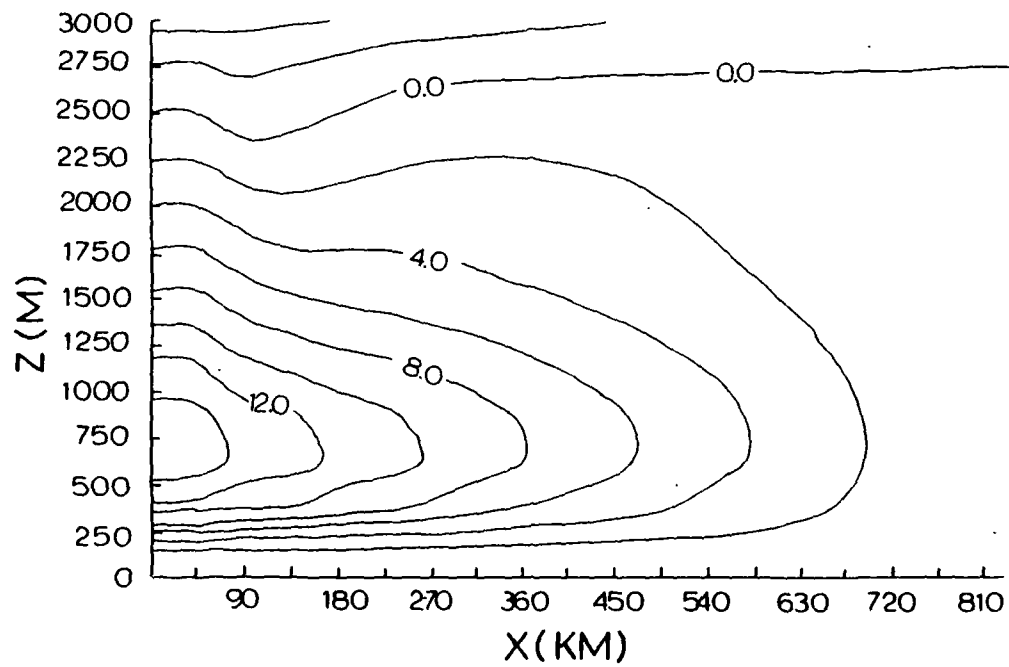


Fig. 9a. Isotach analysis at 28 h for  $v$ .

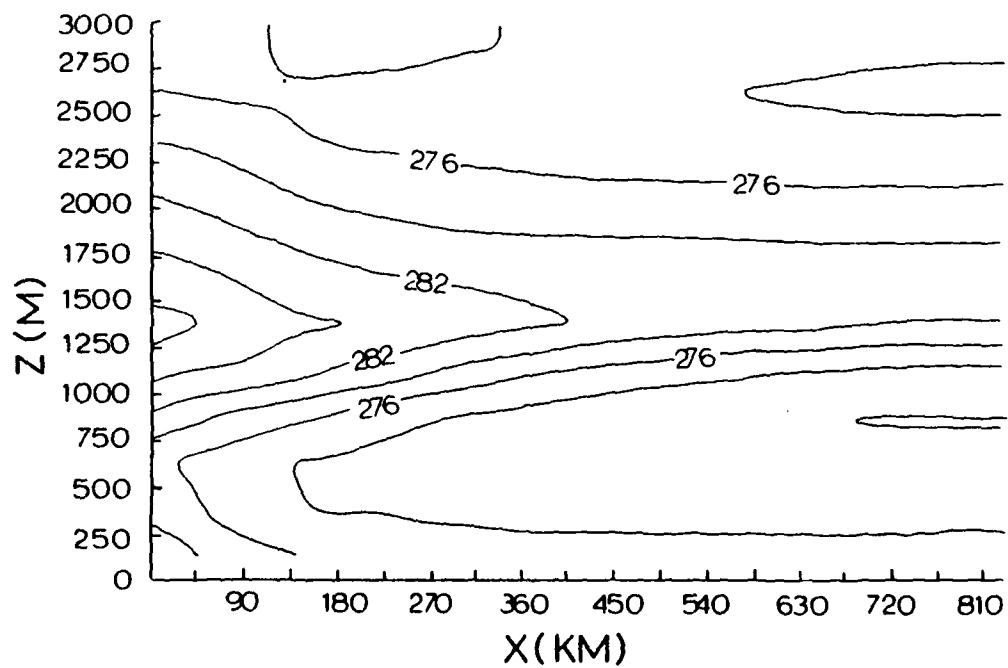


Fig. 9b. Isotherms at 28 h.

wind, while the second figure in each set consists of an  $x - s$  cross section showing an isotherm analysis. Selected isotachs in the first figure of each set are labelled in  $m s^{-1}$ . Selected isotherms in the second figure of each set are labelled in K. The sets of figures are given at intervals of 4 h, beginning with the results at 4 h.

1) Propagation of the low-level jet

Because the coriolis parameter  $f$  was considered constant during the calculation, the  $x$  axis will be considered an axis of constant latitude in the following discussion. For this reason, negative values of  $u$  are referred to as easterly, while positive values of  $v$  are referred to as southerly in the following comments. As shown by the isotach analysis in Fig. 4, a low-level southerly wind develops adjacent to the left boundary where the maximum warming occurs. The maximum value of the wind remains near the left boundary, with the southerly wind speed increasing throughout the integration period. This result is similar to that obtained by Shen (1980), with the exception that the maximum wind value did not show the slight eastward movement obtained by Shen (1980). The maximum value of the wind obtained is less than one-half the value obtained by Shen (1980). This is due to the difference in forcing mechanisms between the

two models discussed earlier. The temperature gradient achieved by the heating mechanism in this model was only about 7 K across the entire domain. The temperature increase at the lowest level on the left hand boundary was about 7 K, less than the heating rate obtained by Shen. Because of the large difference in horizontal temperature gradients obtained in the two models, it is expected that the maximum winds obtained would be less in the present study. While the maximum values obtained are lower, the values of southerly wind produced in the interior of the model are similar, as shown by Fig. 10. Values for the maximum southerly wind obtained by Shen (1980) presented in Fig. 10 are evaluated from the isotach analysis presented in his paper. The numerical scheme used in the present study causes the pressure fall to propagate rapidly across the model domain when the model is heated at the boundary. Attempts were made to achieve horizontal temperature gradients similar to that obtained by Shen (1980) by setting  $Q = 0$  in the interior of the model and heating strongly at the boundary, but it was not possible to achieve as strong a pressure gradient across a small grid interval as did Shen (1980) without excessive heating.

## 2) Subsidence-type inversion

Part b in Figs. 3-9 shows the distribution of

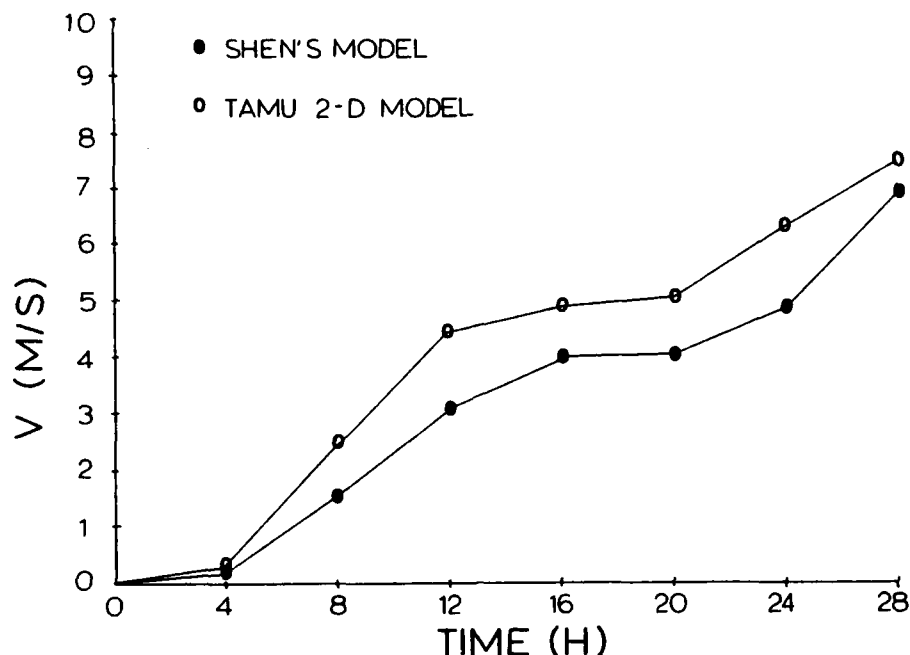


Fig. 10. Comparison of maximum speed of southerly wind 400 km from left hand boundary in Shen's model with TAMU two-dimensional model.

temperature at 4 h intervals, with isotherms labeled in K. These results show the time evolution of a subsidence type inversion very similar to that observed by Shen (1980) in his study. Consistent with his results, the subsidence inversion layer moves downward with time, with the greatest vertical displacement occurring at the left boundary and lesser vertical displacement occurring eastward across the model domain. The strength of the inversion is also noted to decrease slightly in the positive  $x$  direction. As noted by Shen (1980), the occurrence of a subsidence inversion and its importance to the low-level jet have been noted by many investigators,

including Bonner (1966), Beckman (1973), and Damiani (1979). It is significant that the subsidence was sufficient to prevent the inversion from disappearing despite the differential vertical heating applied. Figure 11 shows the distribution of  $\dot{s}$  at 28 hours in  $\text{cm s}^{-1}$ . The result of subsidence occurring throughout the model domain is at first surprising in light of the fact that  $Q$  makes a positive contribution to Richardson's equation. Scale analysis of the individual terms involved shows that near the level of the maximum wind, the term  $-\frac{1}{H} \nabla \cdot \vec{V} H$  is about 1 order of magnitude larger than the other terms in the second integrand. This term makes a negative contribution to vertical motion due to the horizontal divergence of the wind field. The last term is also negative due to the convergence which occurs at the top of the model to satisfy the top boundary condition, and is comparable in magnitude to the other divergent term discussed above. The remaining terms make a positive contribution which is too small to offset the contribution of the negative terms. Setting  $u = 0$  at the left boundary allows the development of a positive vertical motion in the areas where heating is applied because of the horizontal convergence which occurs near the left boundary as the  $x$  component of the wind is forced to slow down. Figure 11 indicates that mass is entering the top of the model to partially compensate for the mass flux through

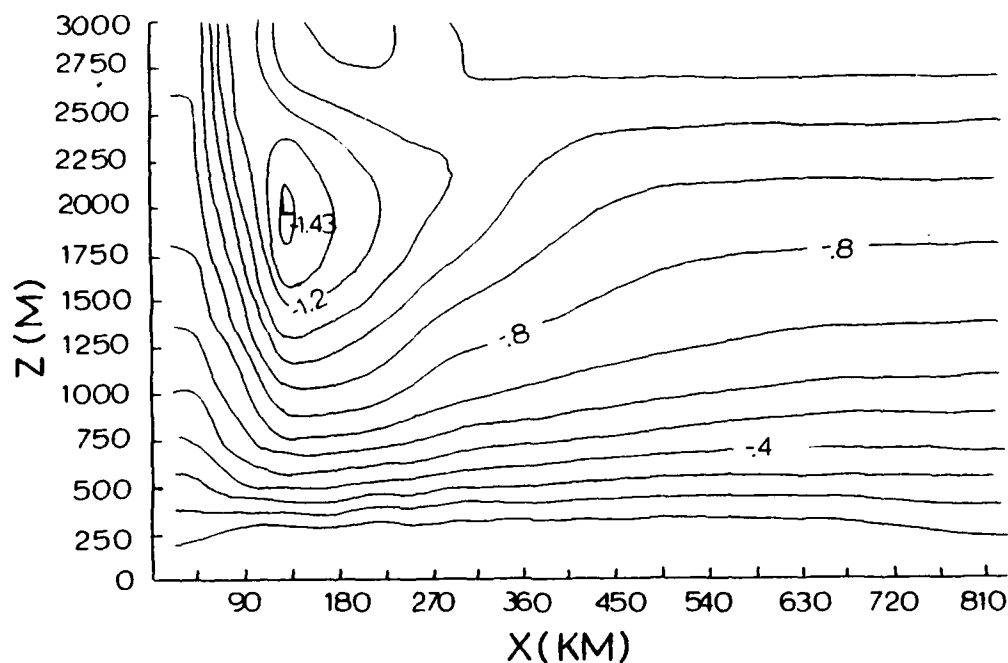


Fig. 11. Vertical motion  $s$  at 28 h in  $\text{cm s}^{-1}$ .

the left boundary, resulting in subsidence throughout the model domain. Figure 12 shows the circulation in the  $x$ - $s$  plane given by the stream function defined by

$$u \approx -\frac{1}{H} \frac{\partial \Psi}{\partial s}, \quad (61)$$

$$s = \frac{1}{H} \frac{\partial \Psi}{\partial x}. \quad (62)$$

The stream function values in Fig. 12 were approximated by integrating (61) from the surface, where the stream function is arbitrarily equal to zero, to the top of the model. A more accurate stream function calculation would involve solving

$$\nabla^2 \Psi = f, \quad (63)$$

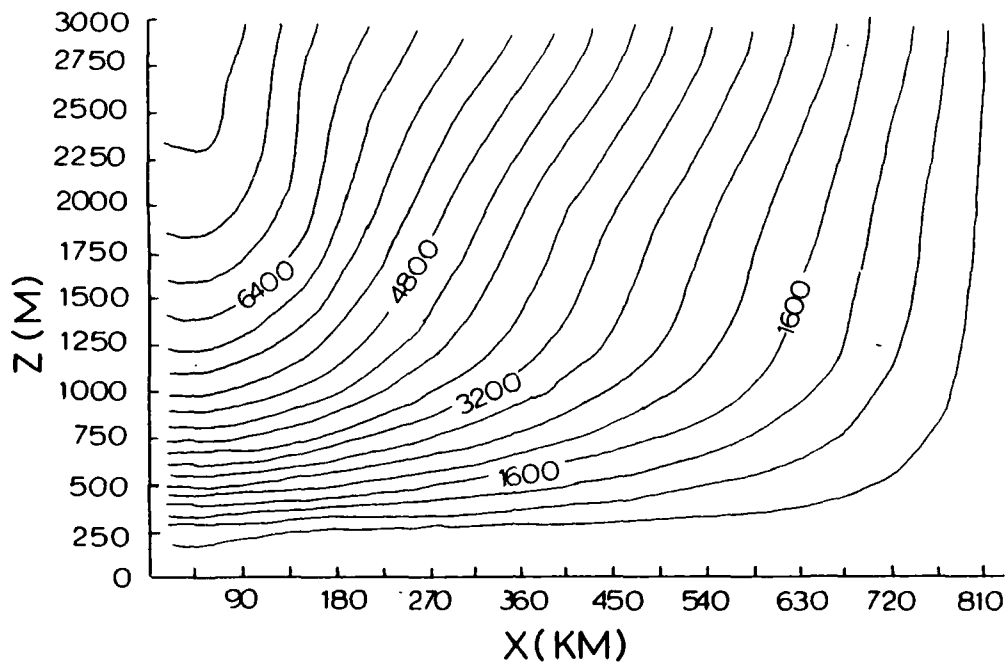


Fig. 12. Streamfunction in  $\text{m}^2\text{s}^{-1}$ .

where  $\zeta = H \frac{\partial \dot{s}}{\partial x} - \frac{1}{H} \frac{\partial u}{\partial s}$  . (64)

Solution of (63) would require boundary conditions for  $\psi$  on all boundaries. The approximate solution given by (61) neglects the nondivergent part of the circulation in the vertical plane. Figure 12 also shows that mass is entering the top of the model and exiting the lower left boundary, in agreement with Fig. 11. Values of  $\dot{s}$  estimated from Fig. 12 by applying (62) are in fair agreement with the calculated values, giving some further justification for the integration of (61) rather than the complete solution of (63).

3) The relation between the low-level jet and the inversion.

As shown by comparison of the isotach and isotherm analyses in Figs. 3-9, the maximum value of the southerly wind occurs just at or below the inversion base in each frame. By 28 h the bottom of the inversion layer is almost coincident with the maximum southerly wind band. As shown in the isotach analyses, the level of the maximum southerly wind increases eastward slightly as the height of the inversion increases eastward spatially. This result also was obtained by Shen (1980). For comparison, a model simulation was also carried out in which the initial conditions were similar with the exception that the initial temperature profile was slightly stable throughout with no inversion layer. The isotachs in the  $x - s$  plane for the southerly component of the wind achieved at 28 h are presented in Fig. 13 in  $m s^{-1}$ . Comparison of these isotachs with those in Fig. 9 b shows that the resulting wind is deeper in the no-inversion case, with a weaker vertical wind shear produced above the level of the maximum wind. The strength of the maximum wind obtained is similar due to the similar forcing mechanism. The only difference which reasonably could be expected concerns the vertical variation of the wind,

which is shown to be quite different in the no inversion case, particularly in the interior region of the model.

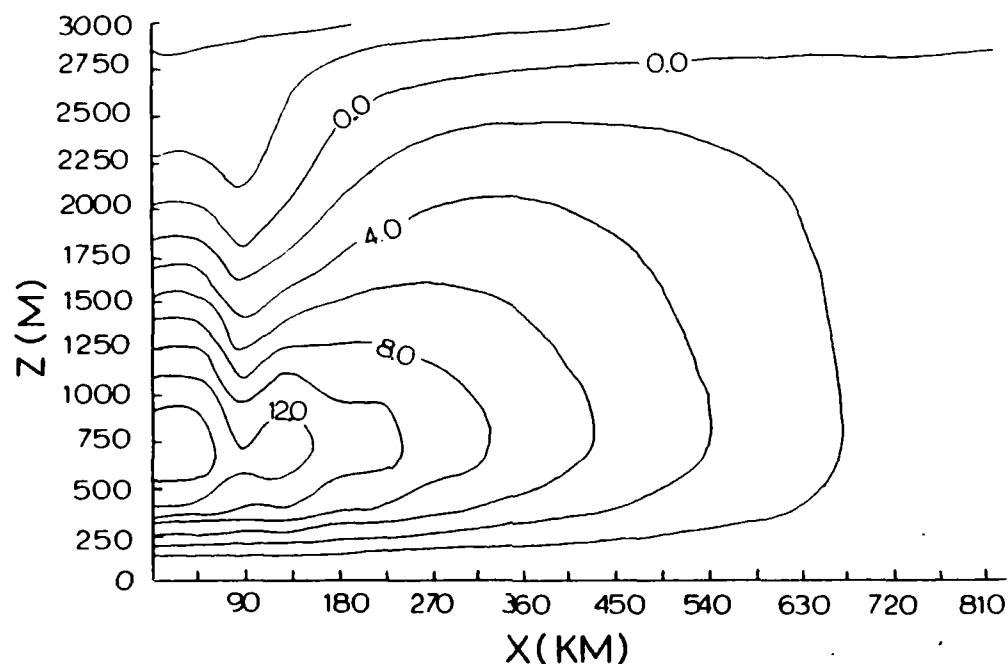


Fig. 13. Isotach analysis at 28 h for v for no inversion case.

4) Quasi-geostrophic adjustment of the southerly flow.

Because pressure is not allowed to vary along the y axis in this study, the u component of the wind is the isallobaric wind. Figure 14 shows the time evolution of the maximum values of the easterly and southerly wind.

These results show that the easterly wind is stronger

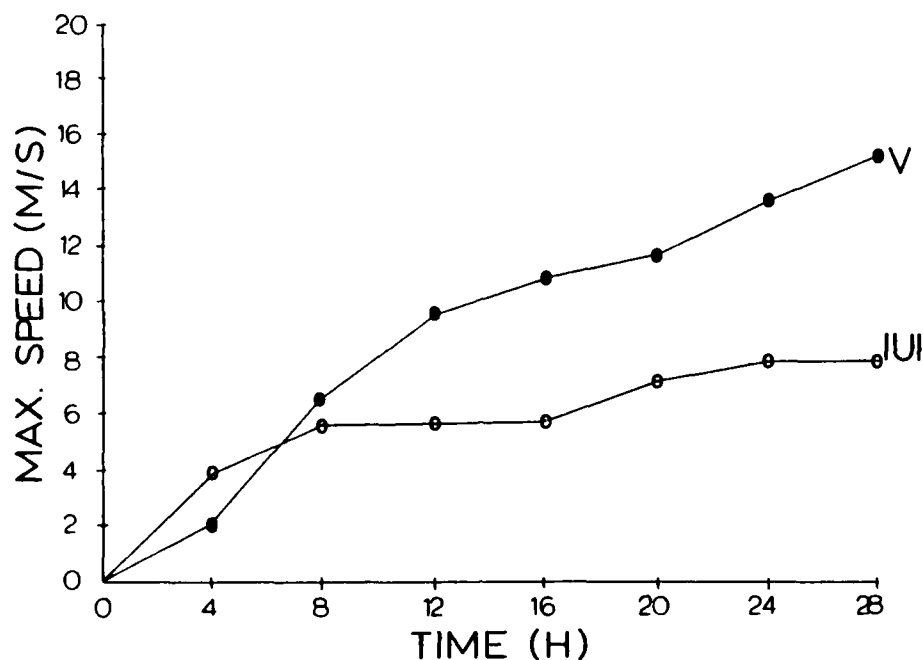


Fig. 14. Time variation of the maximum southerly and easterly wind.

for the first 6 h of the simulation, after which the southerly wind becomes increasingly stronger with time due to the Coriolis effect. The easterly wind appears to become relatively steady after 16 h. These results indicate that the southerly wind becomes increasingly quasi-geostrophic with time during the simulation. The easterly wind does not become increasingly quasi-geostrophic because this would require the development of a pressure gradient in the  $y$  direction which is not allowed in this two-dimensional simulation. Examination

of Figs. 3 - 9 shows that the thermal wind relationship is approximated above the level of the maximum wind, above which the wind decreases with height. This would result in a thermal wind at these levels whose magnitude is less than zero. This is consistent with the warming at the left boundary. Below the level of the maximum wind the surface frictional effects do not allow the thermal wind to be approximated. These results are consistent with the geostrophic adjustment reported by Shen (1980) in his simulation.

## 5. CONCLUSIONS AND RECOMMENDATIONS

As a result of this study, the following conclusions can be made:

1. Conservation of mass is not violated by the finite-difference equations used at interior grid points in this model. Any loss or gain of mass which occurs in the model domain is due to differential flux of mass through the boundaries of the model.
2. Kinetic energy production by the model is slightly lower than that predicted by an analysis of individual terms in the kinetic energy budget. This analysis shows that no spurious kinetic energy is created by the finite-difference equations.
3. The finite-difference scheme is numerically stable for at least 28 h with the parameters used in this study.
4. The results obtained in a simulation of the development of a low-level jet are very similar to those obtained by Shen (1980). The low-level jet showed comparable development and was associated with an inversion which capped the maximum southerly wind. The inversion was maintained by subsidence in the model. The quasi-geostrophic adjustment of the southerly flow was similar in both cases. The model results differed in the strength of the maximum wind due to the different pressure

gradients which were produced as a result of differential heating. A control case involving no inversion showed a deeper wind field with weaker vertical wind shear above the level of maximum wind.

5. The finite-difference equations used in this study were similar to those used in the three-dimensional model of Djuric and Das (1982), except for those used in the advection scheme. In light of the fact that no numerical instabilities occurred in the two-dimensional version used here, it is likely that the difficulties experienced in the three-dimensional model of Djuric and Das (1982) were due to unresolved programming errors, possibly related to the three-dimensional advection scheme. The three-dimensional model used an enstrophy and kinetic energy conserving advection scheme (Djuric and Das, 1982), which was not used in the simplified model presented here because it is not appropriate for a two-dimensional model. The finite-difference forms of Richardson's equation and the density tendency equation used here appear to be sound because they were used successfully. A three-dimensional model incorporating forms of Richardson's equation and the density tendency equation similar to those used here appears feasible if the advection scheme used is carefully formulated.

The following recommendations are made:

1. The model should be improved by adding moisture

to the equations used, with careful attention given to the convective adjustment process.

2. Improvements should be made in the internal friction terms to provide a more realistic simulation in the boundary layer. Also, resolution should be increased in the lower boundary layer.

3. Further testing should be undertaken by incorporating real data into the model to attempt to simulate actual atmospheric processes.

4. Further attempts at modeling of a low-level jet should use more realistic lateral boundary conditions than those used here. In addition, the forcing mechanism should be more physically realistic than that used here or by Shen (1980). Diurnal variations of heating should be included. Such simulations should be three-dimensional if possible.

5. The model should be extended to three dimensions, with careful attention given to the advection scheme used. The validation tests used here should be repeated on the new three dimensional version, followed by verification tests involving real data. Successful completion of such a model would fulfill the requirements of Djuric and Das (1982) given previously.

## REFERENCES

- Anthes, R. A., and T. T. Warner, 1978: Development of hydrodynamic models suitable for air pollution and other mesometeorological studies. Mon. Wea. Rev. 106, 1045-1078.
- Beckman, S. K., 1973: A study of wind maxima near the surface over the south central United States. M.S. Thesis, Texas A&M University, College Station, Texas, 73pp.
- Bonner, W. D., 1966: Case study of the thunderstorm activity in relation to the low-level jet. Mon. Wea. Rev., 94, 167-178.
- Cotton, W. R., and G. J. Tripoli, 1978: Cumulus convection in shear flow - three dimensional numerical experiments. J. Atmos. Sci., 35, 1503-1521.
- Damiani, M. S., 1979: Structure of the low-level jet over Texas. M.S. Thesis, Texas A&M University, College Station, Texas, 97 pp.
- Djuric, D., and P. Das, 1982: Mesoscale Numerical Model. TAMU Texas Hiplex Studies for 1979, Austin, Texas Department of Water Resources, 246-264.
- Fritsch, J. M., and C. F. Chappell, 1980: Numerical prediction of convectively driven mesoscale pressure systems. Part II: Mesoscale model. J. Atmos. Sci., 37, 1734-1762.
- Haltiner, G. J., and R. T. Williams, 1980: Numerical Prediction and Dynamic Meteorology. John Wiley and Sons, 312-313.
- Klemp, J. B., and R. B. Wilhelmson, 1978: The simulation of three-dimensional convective storm dynamics. J. Atmos. Sci., 35, 1070-1096.
- Nickerson, E. C., J. M. Fritsch, C. F. Chappell, and D. R. Smith, 1978: Numerical simulations of orographic and convective cloud systems. NOAA Environ. Res. Lab., Annual Report, Contract No. 8-07-83-V0017, 118 pp.

- \_\_\_\_\_, \_\_\_\_\_, \_\_\_\_\_, and \_\_\_\_\_, 1979: On the numerical simulation of airflow and cloud over mountainous terrain. Contrib. Atmos. Phys., 52, 161-177.
- Orlanski, I., 1975: A rational subdivision of scales for atmospheric processes. Bull. Am. Met. Soc., 56, 527-530.
- Perkey, D. J., 1976: A description and preliminary results from a fine-mesh model for forecasting quantitative precipitation. Mon. Wea. Rev., 104, 1513-1526.
- Pielke, R., 1974: A three-dimensional numerical model of the sea breezes over South Florida. Mon. Wea. Rev., 102, 115-139.
- \_\_\_\_\_, 1976: Models of mesoscale systems. Role of the Gulf of Mexico in the Weather of the United States, a conference on meteorology over and near the Gulf, Jan. 14-16, 1976, Texas A&M University and Amer. Meteor. Soc., 55-67.
- \_\_\_\_\_, 1981: Mesoscale Numerical Modeling. Advances in Geophysics, 23, 285-290.
- Schlesinger, R. E., 1978: A three-dimensional numerical model of an isolated thunderstorm: Part I. Comparative experiments for variable ambient wind shear. J. Atmos. Sci., 35, 690-713.
- Shen, T., 1980: A multiple layer numerical model of the formation of the low-level jet. M.S. Thesis, Dept. of Meteorology, Texas A&M University, 47 pp.
- Tapp, M. C., and P. W. White, 1976: A nonhydrostatic mesoscale model. Quart. J. Roy. Meteor. Soc., 102, 277-296.
- Tripoli, G. J., and W. R. Cotton, 1980: A numerical investigation of several factors contributing to the observed variable intensity of deep convection over South Florida. J. Appl. Meteor., 19, 1037-1063.
- Ullanski, S. L., and M. Garstang, 1978: The role of surface divergence and vorticity in the life cycle of convective rainfall. Part I: observation and analysis. J. Atmos. Sci., 35, 1047-1062.

Warner, T. T., R. A. Anthes, and A. L. McNab, 1978:  
Numerical simulations with a three-dimensional  
mesoscale model. Mon. Wea. Rev. 106, 1079-1099.

## APPENDIX

The following derivations are given by Djuric and Das (1982) and are repeated here for convenience.

a. Derivation of the pressure tendency equation (7)

Differentiation of the hydrostatic equation (3) with respect to time yields:

$$\frac{\partial}{\partial s} \frac{\partial p}{\partial t} = -g H \frac{\partial \rho}{\partial t} \quad (65)$$

Elimination of  $\frac{\partial \rho}{\partial t}$  between (65) and (4) gives:

$$\frac{\partial}{\partial s} \frac{\partial p}{\partial t} = -g H \left( -\nabla \cdot \rho \vec{V} - \frac{\partial}{\partial s} \rho \dot{s} - \frac{\rho}{H} \vec{V} \cdot \nabla H \right) \quad (66)$$

which can be written

$$\frac{\partial}{\partial s} \frac{\partial p}{\partial t} = g \nabla \cdot H \rho \vec{V} + g H \frac{\partial}{\partial s} \rho \dot{s} \quad (67)$$

Integration of (67) from some level  $s$  to the top of the model gives

$$\left( \frac{\partial p}{\partial t} \right)_s = \left( \frac{\partial p}{\partial t} \right)_1 - g \int_s^1 \nabla \cdot H \rho \vec{V} ds + g H \rho \dot{s} - g H \rho_1 \dot{s}_1 \quad (68)$$

which is (7).

b. Derivation of Richardson's equation (9)

The continuity equation (4) can be written

$$\frac{1}{\rho} \frac{\partial \rho}{\partial t} = - \nabla \cdot \vec{V} - \frac{\vec{V}}{\rho} \cdot \nabla \rho - \frac{\partial \dot{s}}{\partial s} - \frac{\dot{s}}{\rho} \frac{\partial \rho}{\partial s} - \frac{1}{H} \vec{V} \cdot \nabla H, \quad (69)$$

or

$$\frac{1}{\rho} \frac{d\rho}{dt} = - \nabla \cdot \vec{V} - \frac{\partial \dot{s}}{\partial s} - \frac{1}{H} \vec{V} \cdot \nabla H. \quad (70)$$

The First Law of Thermodynamics in entropy form is

$$\frac{Q}{C_p T} = \frac{1}{T} \frac{dT}{dt} - \frac{R}{p C_p} \frac{dp}{dt}. \quad (71)$$

Writing the equation of state (6) as

$$\frac{dT}{T} = \frac{dp}{p} - \frac{dp}{\rho} \quad (72)$$

and substituting into (71) gives the result

$$\frac{Q}{C_p T} = - \frac{1}{p} \frac{dp}{dt} - \frac{1}{\rho} \frac{dp}{dt} - \frac{R}{p C_p} \frac{dp}{dt} \quad (73)$$

or

$$\frac{Q}{C_p T} = - \frac{1}{\rho} \frac{dp}{dt} + \frac{1}{p} \frac{dp}{dt} \left( 1 - \frac{R}{C_p} \right). \quad (74)$$

This can be written as

$$\frac{1}{\rho} \frac{dp}{dt} = \frac{1}{\gamma p} \frac{dp}{dt} - \frac{Q}{C_p T}, \quad (75)$$

where  $\gamma = \frac{C_p}{C_v}$ .

Eliminating  $\frac{dp}{dt}$  between (70) and (75) and solving for

$\frac{\partial \dot{s}}{\partial s}$ ,

$$\frac{\partial \dot{s}}{\partial s} = - \frac{1}{\gamma p} \frac{dp}{dt} + \frac{Q}{C_p T} - \frac{1}{H} \vec{V} \cdot \nabla H - \nabla \cdot \vec{V} \quad (76)$$

or

$$\frac{\partial \dot{s}}{\partial s} = -\frac{1}{\gamma p} \frac{dp}{dt} + \frac{Q}{C_p T} - \frac{1}{H} \nabla \cdot H \vec{V} \quad (77)$$

Adding  $\vec{V} \cdot \nabla p + \dot{s} \frac{\partial p}{\partial s}$  to both sides of (68) gives

$$\begin{aligned} \frac{\partial p}{\partial t} + \vec{V} \cdot \nabla p + \dot{s} \frac{\partial p}{\partial s} &= \vec{V} \cdot \nabla p + \left[ \dot{s} \frac{\partial p}{\partial s} \right] - g \int_s^1 \nabla \cdot H \rho \vec{V} ds' + \\ &\left[ g H \rho \dot{s} \right] - g H \rho_1 \dot{s}_1 + \left( \frac{\partial p}{\partial t} \right)_1 \quad (78) \end{aligned}$$

The hydrostatic equation can be used to eliminate the bracketed terms since they cancel one another.

Substituting the result into (77) gives

$$\frac{\partial \dot{s}}{\partial s} = -\frac{\vec{V} \cdot \nabla p}{\gamma p} + \frac{D}{\gamma p} - \frac{1}{\gamma p} \left( \frac{\partial p}{\partial t} \right)_1 + \frac{Q}{C_p T} - \frac{1}{H} \nabla \cdot H \vec{V} \quad (79)$$

where  $D = g \int_s^1 \nabla \cdot H \rho \vec{V} ds'$  and  $g \rho_1 H \dot{s}_1 = 0$  because  $\dot{s}_1 = 0$ .

Integration of (79) gives

$$\dot{s} = \int_0^s \left( \frac{D - \vec{V} \cdot \nabla p}{\gamma p} + \frac{Q}{C_p T} - \frac{1}{H} \nabla \cdot H \vec{V} \right) ds' - \frac{1}{\gamma} \left( \frac{\partial p}{\partial t} \right)_1 \int_0^s \frac{ds'}{p} \quad (80)$$

which is Richardson's equation (9).

#### c. Derivation of equation for pressure tendency at s=1

Application of the top boundary condition  $\dot{s} = 0$  at  $s = 1$  to (80) and rearranging terms gives

$$\left(\frac{\partial p}{\partial t}\right)_1 = \frac{\int_0^1 \left( \frac{D - \vec{\nabla} \cdot \nabla p}{\gamma p} + \frac{Q}{C_p T} - \frac{1}{H} \nabla \cdot H \vec{V} \right) ds}{\int_0^1 \frac{ds}{p}} \quad (81)$$

which is (10).

d. Derivation of density tendency equation.

Eq. (75) can be written

$$\frac{\partial \rho}{\partial t} + \vec{\nabla} \cdot \nabla \rho + \dot{s} \frac{\partial \rho}{\partial s} = \frac{\rho}{\gamma p} \left[ \frac{\partial p}{\partial t} + \vec{\nabla} \cdot \nabla p + \dot{s} \frac{\partial p}{\partial s} \right] - \frac{\rho Q}{C_p T} \quad (82)$$

Substituting (68) into (82) and simplifying using the hydrostatic equation and the top boundary condition gives

$$\frac{\partial \rho}{\partial t} = - \vec{\nabla} \cdot \nabla \rho - \dot{s} \frac{\partial \rho}{\partial s} + \frac{\rho}{p \gamma} \left(\frac{\partial p}{\partial t}\right)_1 - \rho \left[ \frac{D - \vec{\nabla} \cdot \nabla p}{\gamma p} + \frac{Q}{C_p T} \right] \quad (83)$$

which is Eq. (8).

## VITA

Michael Kent Walters was born in Roseburg, Oregon on July 27, 1954, to Mr. and Mrs. Earl O. Walters. He attended public schools in Oregon, Washington, California, and Texas and graduated from Lufkin High School in May, 1972. He completed work for his Bachelor of Science in Zoology at Texas A&M University in December, 1976. In May, 1979, he was commissioned in the United States Air Force. After completing the basic meteorology program at Texas A&M in August, 1980, he was stationed at Air Force Global Weather Central at Offutt Air Force Base, Nebraska. Following completion of his tour at Offutt, he continued his education at Texas A&M University. He is married to the former Sally Ann Brady of Riverside, California. They have two children, Anne and Brian.

The author's permanent mailing address is

106 Lakewind Drive  
Lufkin, Texas 75901

This thesis was typed by the author.

**END**

**FILMED**

**12-85**

**DTIC**